Towards a mechanistic model of plankton population dynamics

Mark E.Baird and Steve M.Emsley

Ecosystems Analysis and Management Group, Department of Biological Sciences, University of Warwick, Coventry CV4 7AL, UK

Abstract. A plankton population model is developed from literature studies with mechanistic descriptions of interactions of individual plankton cells. Interactions considered include diffusion and convection of nutrients to phytoplankton cell surfaces, light capture by phytoplankton pigment assemblages, sinking rates of phytoplankton cells, and encounter rates of predators and prey. Mechanistic formulations are based on individual species characteristics, obtained from measurements in laboratory experiments, and are functions of local fluid properties such as small-scale turbulence and viscosity. Phytoplankton growth is modelled by analogy to chemical kinetics, and is a function of intracellular nutrient and energy reserves. Results from laboratory experiments on single-species populations found in the literature are used to test the applicability of the functional forms for quantifying interactions of populations of common marine plankton species. These functional forms are then used to construct a system of equations describing plankton population dynamics. Simulations of plankton population dynamics at environmental conditions similar to the oceanic mixed layer at Bermuda (32°N, 65°W) and Ocean Weather Station (OWS) 'India' (59°N, 19°W) are performed, and compared to existing models and field data sets.

Introduction

Plankton population modelling has traditionally been based on simple empirical models (Steele and Henderson, 1981), without detailed theoretical consideration of the underlying physical processes involved. Empirical models usually capture the dynamics of a few chosen phenomena, such as the spring bloom (Taylor and Stephens, 1993), predator–prey interactions (Edwards and Brindley, 1996) or recycling of nitrate (Fasham *et al.*, 1990). However, empirical models have been unable to describe the range of phenomena necessary to become useful tools for forecasting geochemical quantities and biological populations in natural ecosystems (Botsford *et al.*, 1997). Recently, some global climate models have achieved greater accuracy in forecasting, by employing explicit physical laws, rather than empirical relationships based on historical data sets (Kerr, 1998; Stockdale *et al.*, 1998). Could such a theoretical approach improve the forecasting of biological populations?

A large number of theoretically derived, and empirically tested, mechanistic and semi-empirical functional forms (Table I defines the terms mechanistic, semi-empirical, empirical and heuristic) relevant to modelling plankton populations are described in the literature (Pasciak and Gavis, 1975; Kirk, 1975a; Gerritsen and Strickler, 1977; Brock, 1981; Mellor and Yamada, 1982; Rothschild and Osborn, 1988; Blanchard, 1989; Jackson, 1995; Blake and Otto, 1996; Karp-Boss *et al.*, 1996; Pahlow *et al.*, 1997). In the last decade, modellers have used mechanistic light (Fasham *et al.*, 1990), semi-empirical aggregation (Jackson and Lochmann, 1992) and mixing (Sharples and Tett, 1994) functions to describe environmental forcings in plankton population models. By considering an isolated mechanism in detail, these studies have given ecologists an insight into

Table I. Definition of adjectives describing the method of determining functional forms

Adjective	Description
Mechanistic	Formulae based on theoretical consideration of underlying physical processes only
Semi-empirical	Formulae based on theoretical considerations, with experimentally determined constants
Empirical	Formulae based on experimental data only
Heuristic	Intuitively determined formulae based on endpoints and chosen from simple functional forms

what effects a particular mechanism may have on population dynamics. However, so far, modellers have not attempted to incorporate mechanistic functional forms into the biological processes in a plankton population model.

The major obstacle to incorporating mechanistic functional forms into plankton population models is the quantification of phytoplankton and zooplankton in terms of total biomass of phytoplankton and zooplankton species, respectively. By using a plankton population model structure based on populations of individual plankton cells, mechanistic interactions can be considered, with constants derived from controlled laboratory experiments. Laboratory-determined constants typically have greater precision than field measurements, and their use in mechanistic functional forms allows explicit quantification of the effects of environmental variables, such as small-scale turbulence and viscosity, on population dynamics. The resulting model should provide a general description of plankton population dynamics in a variety of environments.

The aim of this paper is to develop, as far as possible, a plankton population model based on theoretically derived functional forms and laboratory-determined constants. This has necessitated functional forms describing interactions of individual plankton cells. The mechanistic functional forms are then compared to the literature describing the dynamics of populations of single plankton species in the laboratory environment. These comparisons evaluate the usefulness of functional forms, based on individual cells, in describing population dynamics. The model equations are then combined and simulations of plankton population dynamics in the oceanic mixed layer at Bermuda and Ocean Weather Station (OWS) 'India' are performed, and compared to other models (Fasham *et al*., 1990; Fasham, 1993) and field data sets.

The model

Model structure

The model structure is based on a series of ordinary differential equations (ODEs) describing the interactions of individual plankton species. With the processes described in words, the ODEs are:

$$\frac{dN_i}{dt} = \text{– nutrient uptake + nutrient recycled} \tag{1}$$

$$\frac{dQ_{i,j}}{dt} = \text{nutrient uptake – nutrient for growth} \tag{2}$$

$$\frac{dq_j}{dt} = \text{light captured – energy for growth} \tag{3}$$

$$\frac{dP_j}{dt} = \text{+ growth – sinking – grazing loss} \tag{4}$$

$$\frac{dH_k}{dt} = \text{+ grazing uptake} \tag{5}$$

where N_i is the extracellular nutrient concentration of chemical species i [mol (N_i) m^{-3}], $Q_{i,j}$ is the internal cell quota of nutrient i, in phytoplankton species j [mol (Q_i) cell $(P_j)^{-1}$], q_j is the internal cell quota of energy, in phytoplankton species j [mol (q) cell $(P_j)^{-1}$], P_j is the concentration of phytoplankton species j [mol (P_j) m^{-3}] and H_k is the concentration of herbivore species k [mol (H_k) m^{-3}].

The functional forms describing each process in equations (1–5) must now be selected, and later validated by comparison with experiments in the literature. The implications of mixing of the above quantities, as described by partial differential equations, are also briefly examined.

Nutrient uptake by phytoplankton

The most common functional form chosen by plankton population modellers to describe nutrient uptake is a rectangular hyperbola (Dugdale, 1967):

$$J = \frac{aC_b}{b + C_b} \tag{6}$$

where C_b is the average extracellular nutrient concentration (mol m^{-3}), b is the extracellular nutrient concentration at half the maximum uptake rate (mol m^{-3}) and a is the maximum uptake rate (mol cell^{-1} s^{-1}). However, in addition to extracellular nutrient concentration, nutrient uptake by phytoplankton is also dependent on extracellular physical conditions, such as fluid motion, molecular diffusivity of the nutrient and phytoplankton shape (Pasciak and Gavis, 1975), and intracellular conditions, such as internal nutrient quotas and rates of biochemical reactions (Droop, 1968). To choose a more theoretical functional form for nutrient uptake by phytoplankton, the equations describing extracellular and intracellular uptake processes need to be considered separately, and then solved simultaneously.

Extracellular processes. Nutrient uptake to a single phytoplankton cell, J (mol cell^{-1} s^{-1}), can be determined mechanistically by:

$$J = \psi\, D\, (C_b - C_w) \tag{7}$$

where ψ is the diffusion shape factor (m) (Table II), D is the molecular diffusivity of the nutrient ($m^2\ s^{-1}$), C_b is the average extracellular nutrient concentration (mol m^{-3}) and C_w is the concentration at the wall of the cell (mol m^{-3}). A semi-empirical correction to equation (7), to account for fluid motion around the cell, is provided by the Sherwood number, Sh (dimensionless) (Table III). Sh is a relative measure of the additional flux of nutrient due to the motion of fluid surrounding the cell:

$$Sh = \frac{\text{total flux}}{\text{diffusive flux}} \tag{8}$$

So equation (7) becomes the semi-empirical formula:

$$J = \psi\, DSh\, (C_b - C_w) \tag{9}$$

Table II. Diffusion shape factor ψ (m). ψ is obtained by solving the Laplace equation, $\nabla^2 C = 0$, and the flux at the surface of the cell, $J = \psi D \triangle C$ [equation (9)], where D = molecular diffusivity and $\triangle C$ = concentration difference between the average fluid and the cell wall; $r_{1,2,3}$ are orthogonal radii (m); ψ for an arbitrary shape is $\geq \psi$ of a sphere of same volume, and $\leq$ to ψ of a shape which circumscribes it (Clift *et al.*, 1978). Clift *et al.* (1978) also give solutions for touching and intersecting spheres, cubes, rectangular plates and needle-like bodies. In the case where surface uptake mechanisms are much faster than diffusion to the cell surface, ψ determines the relative ability of a shape to transport mass

Shape	Diffusion shape factor ψ (m)	Reference
Sphere	$4\pi r_1$	LM89
Oblate spheroid		
$r_1 = r_2\ r_2 > r_3$	$4\pi r_1 e \left(\dfrac{1}{\tan^{-1}\frac{e}{\sqrt{1-e^2}}} \right)$ where $e = \sqrt{1 - \left(\dfrac{r_3}{r_1}\right)^2}$	PG75
Prolate spheroid		
$r_1 > r_2\ r_2 = r_3$	$8\pi r_1 e \left(\dfrac{1}{\ln\frac{1+e}{1-e}} \right)$ where $e = \sqrt{1 - \left(\dfrac{r_3}{r_1}\right)^2}$	PG75
General ellipsoid	$\dfrac{I_1}{I_2}$	WR97
$r_1 > r_2 > r_3$	$I_1 = 8 \displaystyle\int_B^C \int_0^B \frac{\theta^2 - \lambda^2}{\sqrt{(\theta^2 - B^2)\,(C^2 - \theta^2)\,(B^2 - \lambda^2)\,(C^2 - \lambda^2)}}\, d\lambda d\theta$	
	$I_2 = \displaystyle\int_{r_1}^{\infty} \frac{1}{\sqrt{(x^2 - B^2)\,(x^2 - C^2)}}\, dx$	
	$B = \sqrt{r_1^2 - r_2^2},\ C = \sqrt{r_1^2 - r_3^2}$	
Cylinder		
$0 \leq \frac{L}{d} \leq 8$	$\left(8 + 6.95 \left(\dfrac{L}{d}\right)^{0.76} \right) r_1$	CGW78

LM89, Lazier and Mann (1989); PG75, Pasciak and Gavis (1975); WR97, Wolf-Gladrow and Riebesell (1997); CGW78, Clift *et al.* (1978).

Table III. Sherwood numbers, *Sh* (dimensionless), for spheres and other shapes (Brenner, 1963; Karp-Boss *et al.*, 1996; Pahlow *et al.*, 1997). r_1, r_2, r_3 are orthogonal radii (m); r_c = characteristic radii (m), used for non-spherical shapes, and taken to be the radius of a sphere with the same surface area as the non-spherical shape; ψ = diffusion shape factor (m) (Table II); f = dimensionless drag; C_D = drag coefficient (Table V); μ = dynamic viscosity (kg s^{-1} m^{-1}); K_D = Kolmogorov length scale for diffusion (m); v = kinematic viscosity (m^2 s^{-1}); E = shear rate (s^{-1}); ϵ = mean rate of dissipation of turbulent kinetic energy (m^2 s^{-3}); D = molecular diffusivity of transferred chemical species (m^2 s^{-1}); Pe = Peclet number = $\dfrac{r_1^2 \epsilon^{0.5}}{D v^{0.5}}$; Re = Reynolds number = $\dfrac{r_1^2 \epsilon^{0.5}}{v^{1.5}}$; U_{rel} = velocity of cell relative to fluid as a result of sinking and swimming from equation (42) (m s^{-1}). For uniform motion in a shear flow, it has been shown for a cylinder at low Re that $Sh = Sh_{shear} + Sh_{uniform}$ (Dabros *et al.*, 1984), and this is assumed true for all shapes. For combinations of shapes and flow regimes not covered, Sh is given by the Sh of a sphere of the same equivalent surface area as the non-spherical shape by substituting r_c for r_1 in the second column

Flow regime	Sphere	Other shapes
Uniform flow	$Sh = 0.5\left(1 + \sqrt[3]{1 + 2Pe}\right)$	$Sh = 1 + 0.5 Sh_0 Pe$
fluid motion due to cell	$Pe = \dfrac{U_{rel} r_1}{D}$	$+0.5 Sh_0 f Pe^2 \ln Pe$
swimming only $\epsilon = 0$		where $Sh_0 = \dfrac{\psi_{shape}}{\psi_{sphere, = SA}}$
		$f = \dfrac{C_D}{6\pi\mu\, r_c} \quad Pe = \dfrac{r_c U_{rel}}{D}$
Shear flow	$Pe < 0.1 \; Sh = 1 + 0.23 Pe^{0.5}$	Prolate sp, $0.1 < Pe < 10$
turbulent-induced shear	$0.1 < Pe < 100 \; Sh = 1.002 + 0.21 Pe^{0.5}$	$Sh = 1 + 0.363 \sqrt{\dfrac{Pe}{r_a + 1}}$
$r_1 < K_D$	$Pe > 100 \; Sh = 0.67 Pe^{1/3}$	$+0.115\, \dfrac{r_a - 1}{r_a + 1}\, Pe^{1/3}$
$K_D = \sqrt[4]{\dfrac{vD^2}{\epsilon}}$	$Pe = \dfrac{E r_1^2}{D} \quad E = 0.71\left(\dfrac{\epsilon}{v}\right)^{1/2}$	$r_a = \dfrac{r_1}{r_3}, \; Pe = \dfrac{E r_a r_3^2}{D}$
Turbulent flow	$Sh = \alpha\, [A + B]^{1/6}$	
turbulent-induced shear	$A = 2.25\left(\dfrac{r_1 U_{rel}}{D}\right)^2$	No literature studies
$r_1 > K_D$	$B = 5.1 S^2 \left(\dfrac{r_1^2}{D}\left(\dfrac{\epsilon}{v}\right)^{0.5}\right)^2$	
$K_D = \sqrt[4]{\dfrac{vD^2}{\epsilon}}$	$0.495 < S < 0.545$	

Intracellular processes. The dependence of uptake on intracellular nutrient concentration has also been recognized, and the concept of an internal cell quota, Q (mol cell^{-1}), introduced (Droop, 1968). One heuristic formulation used to describe the dependence of uptake on internal cell quota is (Sharples and Tett, 1994):

$$J = \Theta\left(\frac{Q^{max} - Q}{Q^{max}}\right) \tag{10}$$

where Θ is a function of other internal and external processes affecting uptake. However, it is clear that internal cell quota only directly affects the intracellular

processes, which themselves must be given a functional form. A common heuristic choice for describing internal cell processes involved in uptake is the rectangular hyperbola [equation (6)], primarily because of its use to describe enzyme kinetics mechanistically (Kuchel and Ralston, 1988), which is often implicated in intracellular uptake processes. This takes the form:

$$J = \frac{VC_w}{K + C_w} \tag{11}$$

where V is the maximum uptake rate of internal processes and K is the nutrient concentration at the cell wall at half the maximum uptake rate of internal processes. Since it is probably the rate of reaction, rather than maximum uptake potential of the internal cell processes, which is a function of internal cell quota, it is assumed that K in equation (11) is the following function of Q:

$$K = K_o \left(\frac{Q^{max}}{Q^{max} - Q} \right) \tag{12}$$

where K_o is the value of K at $Q = 0$. This form was chosen heuristically, based on the simplest function that met the criteria that K approaches infinity at $Q = Q^{max}$, and $K = K_o$ at $Q = 0$. The rate of uptake due to intracellular processes can now be given by:

$$J = \frac{VC_w}{K_o \dfrac{Q^{max}}{Q^{max} - Q} + C_w} \tag{13}$$

Enzyme-mediated uptake has been identified on the surface of cells (Dyhrman and Palenik, 1997). The reaction rate of such enzyme reactions will be dependent on concentration at the cell wall, C_w, and their activity, K, on the cell nutrient status, Q. In the formulation of nutrient uptake presented in this paper, the effects of surface enzyme reactions are included in the internal processes. In fact, equation (13) approximates a series of biochemical reactions and transport processes, from those on the surface, through the cell membrane, to the point of storage within the cell.

Uptake rate, incorporating both extracellular and intracellular processes. Up to this point, both extracellular and intracellular uptake rates have been calculated independently as a function of the concentration of the nutrient at the surface of the cell, C_w. There is no direct way of determining C_w. However, by mass balance, extracellular and intracellular uptake rates must be equal, so by solving simultaneous equations [equations (9) and (13)] (Hill and Whittingham, 1955; Pasciak and Gavis, 1975; Mierle, 1985b), the uptake rate as a function of extracellular nutrient concentration, fluid motion, phytoplankton shape, internal cell quota, and enzyme saturation rate and maximum activity is given by solving the quadratic:

$$\frac{J^2}{\psi DSh} - \left(K_o \left(\frac{Q^{max}}{Q^{max} - Q} \right) + C_b + \frac{V}{\psi DSh} \right) J + VC_b = 0 \qquad (14)$$

Equation (14) is impractical to use for most species, since almost all literature values for K_o and V are determined using equation (6) rather than equation (11). However, an approximation (see below) of equation (14) is achieved by considering the physiological state of the cell directly in equation (9) using equation (10):

$$J_{i,j} = \psi_j D_i Sh_{i,j} N_i \left(\frac{Q_{i,j}^{max} - Q_{i,j}}{Q_{i,j}^{max}} \right) = \left(\frac{dQ_{i,j}}{dt} \right)_{uptake} \qquad (15)$$

where $J_{i,j}$ is the uptake rate of nutrient i to phytoplankton species j [mol (N_i) cell^{-1} s^{-1}], ψ_j is the diffusion shape factor for phytoplankton species j (m) (Table II), D_i is the molecular diffusivity of chemical species i (m^2 s^{-1}) (Table VIII), N_i is the average concentration of chemical species i in the surrounding fluid (mol m^{-3}), $Sh_{i,j}$ is the Sherwood number (Table III) and is a measure of the additional flux of chemical species i to phytoplankton species j due to local fluid motion, $Q_{i,j}$ is the internal cell quota of chemical species i in phytoplankton species j [mol (Q_i) cell (P_j)$^{-1}$] and $Q_{i,j}^{max}$ is the maximum internal cell quota of chemical species i in phytoplankton species j [mol (Q_i) cell (P_j)$^{-1}$] (Table XIII).

Light capture

Phytoplankton absorb incident light as a function of wavelength, pigment concentrations, cell geometry (Kirk, 1994) and the presence of other attenuating components of the water column. The spectrum of absorption coefficients for the pigment assemblage that is characteristic of each phytoplankton species is determined, and then the absorption characteristics of a phytoplankton cell can be calculated depending on the pathlength of light through the cell as a function of cell size, shape and orientation. For cells evenly distributed through a well-mixed layer, light capture by an individual cell will be a function of the incident light on the top of the layer, and the absorption coefficients of all attenuating elements of the medium.

The spectrum of absorption coefficients for a pigment assemblage can be empirically determined by approximating the absorption bands of each pigment as a Gaussian curve (Figure 1), and summing the combined absorption of all bands at each wavelength (Hoepffner and Sathyendranath, 1991). The absorption coefficient at a wavelength λ (nm) due to pigments 1, ..., Y, $(\overline{\gamma C})_\lambda$ (m^{-1}), is given by:

$$(\overline{\gamma C})_\lambda = \sum_{\xi=1}^{Y} \gamma_\xi C_\xi \exp \left(- \frac{(\lambda - \lambda_\xi)^2}{2W_\xi^2} \right) \qquad (16)$$

where C_ξ [mg (pig) m^{-3}] is the concentration of pigment ξ, γ_ξ [m^2 mg (pig)$^{-1}$] is the peak pigment-specific absorption coefficient of the pigment responsible for the ξth Gaussian band, λ_ξ (nm) is the wavelength of maximum absorption and W_ξ (nm) is the halfwidth of the ξth band.
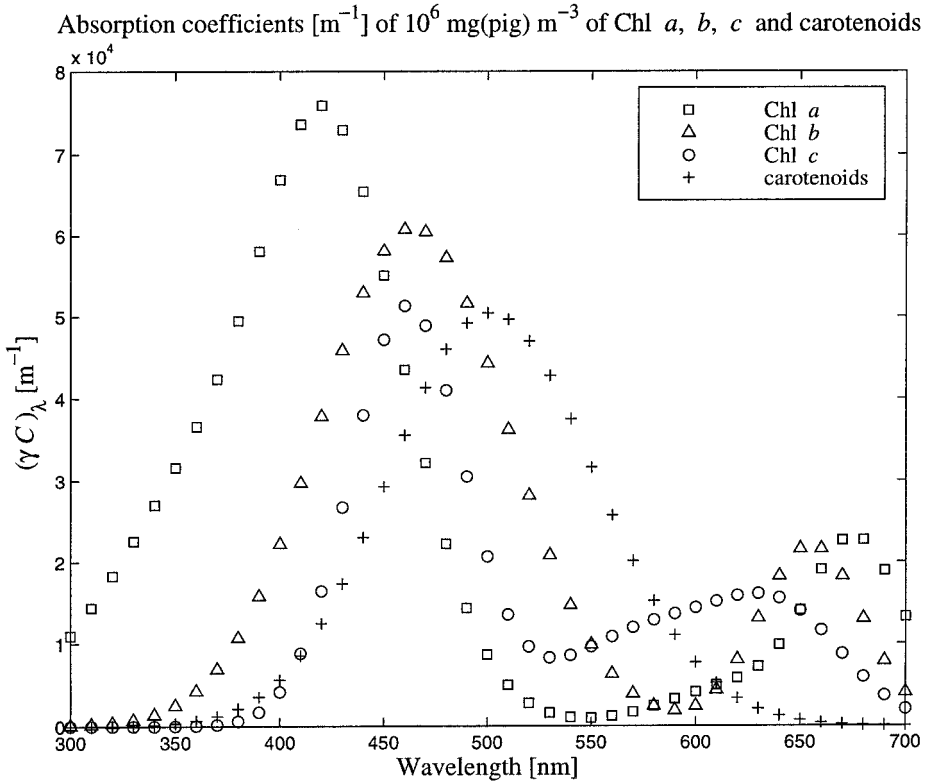
Absorption coefficients $[m^{-1}]$ of 10^6 mg(pig) m^{-3} of Chl a, b, c and carotenoids

Fig. 1. Absorption coefficients, γC_λ (m^{-1}), of 1×10^6 mg (pig) m^{-3} of Chl a ($\square$), Chl b ($\triangle$), Chl c ($\bigcirc$) and carotenoids (+) as approximated by Gaussian curves (Hoepffner and Sathyendranath, 1991). Total absorbance is calculated as the sum of the absorption coefficients due to each pigment at each wavelength [equation (16)].

The pathlength, and therefore light attenuated, of a light beam through a cell is a function of cell shape and orientation with respect to the direction of the beam propagation (Figure 2). The light attenuated by one cell of phytoplankton species j at wavelength λ, $(I_{j,\lambda})_{light\ attenuated}$, is given by (Kirk, 1975a):

$$(I_{j,\lambda})_{light\ attenuated} = a_{j,\lambda}A_j\,(I_\lambda)_{incident\ on\ j} \qquad (17)$$

where $(I_\lambda)_{incident\ on\ j}$ is the incident radiation at wavelength λ on cell j [mol (quanta) m^{-2} s^{-1} nm^{-1}], A_j is the projected area of j on a plane perpendicular to the beam (m^2) and $a_{j,\lambda}$ is the fraction of light absorbed by a cell of species j, at wavelength λ (dimensionless), and is a function of pathlength and $(\overline{\gamma C})_{j,\lambda}$. The product, $a_{j,\lambda}A_j$, is the absorption cross-section of cell j at wavelength λ (m^2). Since both $a_{j,\lambda}$ and A_j vary with shape and orientation, it is simplest to determine the product, $\overline{aA}_{j,\lambda}$, for different cells and orientations. $\overline{aA}_{j,\lambda}$ can be measured in the laboratory for a
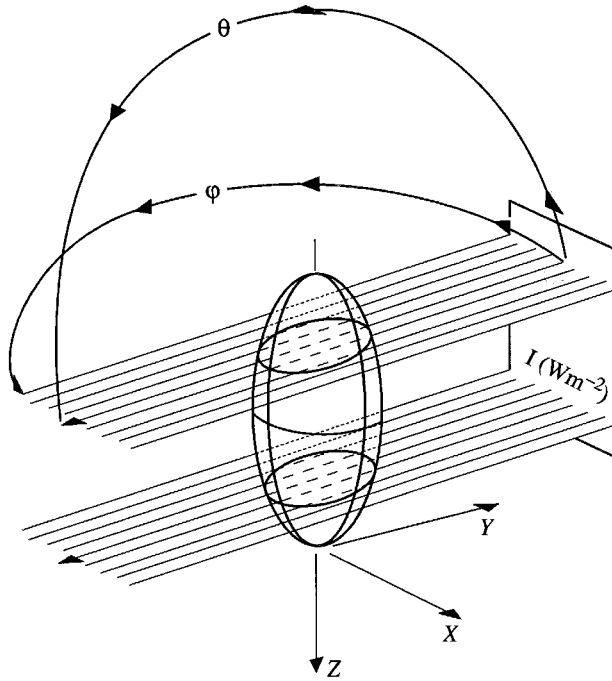
Fig. 2. The pathlength of two planes of light beams through a prolate spheroid. (— , · · ·) Light beam travelling through fluid, in view and behind the spheroid, respectively; (- - -) light beam travelling through the cell. Calculation of the light absorbed by a randomly orientated shape requires determination of the pathlength of light through the cell for all orientations (θ, φ) to the light field, and at each infinitesimally small area of the projected area perpendicular to the beam (in the *XZ* plane) (Kirk, 1975a,b, 1976). In the case of a surface of revolution such as the above prolate spheroid, integration with respect to the angle through which the shape has been revolved (φ above) is not required (Table IV).

particular species adapted to a particular light regime (Lewis *et al.*, 1988), or solved geometrically as a function of shape, pigment concentration and orientation. For the geometric solution, small phytoplankton cells in a turbulent environment cannot control their orientation, so a random orientation with respect to the incident light is assumed. $\overline{aA}_{j,\lambda}$ is determined by considering the light attenuated in each infinitesimally small area of the projected area perpendicular to the beam (in the *XZ* plane in Figure 2) for all orientations (θ, φ in Figure 2) (Table IV). Geometric solution of $\overline{aA}_{j,\lambda}$ allows theoretical investigation of the effect of varying pigment concentrations and shape on light capture.

The incident light on cell *j*, $I_{incident\ on\ j}$, required in equation (17) is a function of incident light on the top [at depth *z* (m)] of the medium, $I_{z,\lambda}$ [mol (quanta) m^{-2} s^{-1} nm^{-1}], the effect of all attenuating components in the medium, and the pathlength through the medium to reach cell *j*. To solve for $(I_{j,\lambda})_{light\ attenuated}$ a well-mixed medium in which all attenuating components are evenly distributed (which

for a cell means it has equal probability of being at any depth in the medium) is assumed. Beer's law (Kirk, 1975a) can now be used to calculate the radiation at the bottom [depth $z - M$ (m)] of the medium, $I_{z-M,\lambda}$ [mol (quanta) m^{-2} s^{-1} nm^{-1}]:

$$I_{z-M,\lambda} = I_{z,\lambda} e^{(-\sum_{x=1}^{X} k_{x,\lambda}) M_{path,\lambda}} \tag{18}$$

where $I_{z-M,\lambda}$ is the radiation at depth $z - M$ (m) after travelling M_{path} (m) through the medium, and $\sum_{x=1}^{X} k$ is the sum of all (X in number) absorbing components of the medium. For water containing humic substances and phytoplankton species, P_j, $j = 1, \ldots, p$, equation (18) becomes:

$$I_{z-M,\lambda} = I_{z,\lambda} e^{-(k_{w,\lambda} + k_{g,\lambda} + \sum_{j=1}^{p} A_v P_j \overline{aA}_{j,\lambda}) M_{path,\lambda}} \tag{19}$$

where $k_{w,\lambda}$ is the partial attenuation coefficient due to pure water at wavelength λ (m^{-1}) (Figure 3), $k_{g,\lambda}$ is the partial attenuation coefficient due to the presence of gilvin or humic substances at wavelength λ (m^{-1}) (Figure 3) and $A_v P_j \overline{aA}_{j,\lambda}$ is the partial attenuation of species j at wavelength λ (m^{-1}) (Kirk, 1975a), where A_v is the Avogadro constant $= 6.02214 \times 10^{23}$ cell mol^{-1} (Atkins, 1994), p is the number of phytoplankton species, $A_v P_j$ is the concentration of phytoplankton species j (cell m^{-3}) and $M_{path,\lambda}$ is the average pathlength of a photon at wavelength λ through the layer (m). If there is no scattering or backscattering of light within

Table IV. Absorption cross-section of randomly orientated phytoplankton cells of a given shape. $A =$ projected area of the cell perpendicular to the light beam (m^2); $a =$ fraction of light absorbed by the cell (dimensionless); $\gamma =$ pigment-specific absorbance [m^2 mg (pig)$^{-1}$]; $C =$ pigment concentration [mg (pig) m^{-3}]; $\overline{\gamma C} =$ the absorption coefficient of all pigments (m^{-1}); $\overline{aA} =$ average absorption cross-section for a randomly orientated cell (m^2); $r_{1,2,3} =$ orthogonal radii of sphere, ellipsoid or cylinder (m); $h =$ height of cylinder (m). For a weakly absorbing particle of any shape, $\overline{aA} = \overline{\gamma C} V$, where $V =$ volume (m^3)

Shape	Absorption cross-section for random orientation, $\overline{aA}$ (m^2)	Reference
Sphere	$\pi r_1^2 \left(1 - \dfrac{2 \left(1 - (1 + 2\overline{\gamma C} r_1) \, e^{-2\overline{\gamma C} r_1} \right)}{(2\overline{\gamma C} r_1)^2} \right)$	Kirk (1975b)
Spheroid	$\displaystyle\int_0^{\pi/2} \pi L v \cos\theta \left(1 - \frac{4}{\pi L v} \int_0^s \int_0^L e^{-2\overline{\gamma C} R} \sqrt{1 - \frac{Z^2}{s^2}} \, dX dZ \right) d\theta$	Kirk (1976)
$r_1 \geq r_2 \geq r_3$	$L = \sqrt{w^2 \cos^2\theta + v^2 \sin^2\theta}$	
	$s = v \sqrt{1 - \dfrac{X^2}{L^2}}$	
	$R = \dfrac{wv \sqrt{v^2 + w^2 \cot^2\theta - X^2 \csc^2\theta}}{\sin\theta \, (v^2 + w^2 \cot^2\theta)}$	
	prolate spheroid $r_1 = w \quad r_2 = r_3 = v$	
	oblate spheroid $r_1 = r_2 = v \quad r_3 = w$	
Cylinder	$\displaystyle\int_0^{\pi/2} 2 r_1 h \cos^2\theta \left(1 - \frac{1}{r_1} \int_0^{r_1} e^{-2\overline{\gamma C} r_1 \sec\theta \sqrt{\left(1 - \frac{Z^2}{r_1^2}\right)}} \, dZ \right) d\theta$	Kirk (1976)

the medium, $M_{path,\lambda} = M \sec \theta$, where θ is the azimuth angle of light propagating through the water, and M_{path} is independent of wavelength.

To determine the fraction of light absorbed by each attenuating component of the medium, we rewrite Beer's law [equation (18)] as:

$$I_{z-M,\lambda} = I_{z,\lambda} \prod_{x=1}^{X} e^{-k_{x,\lambda}} \qquad (20)$$

In a well-mixed medium, with attenuating components spread evenly throughout the medium, the fraction attenuated by one component, $x = \zeta$, out of X components is given by:

$$\frac{e^{-k_{\zeta,\lambda}}}{\sum_{x=1}^{X} e^{-k_{x,\lambda}}} = \frac{-k_{\zeta,\lambda}}{\sum_{x=1}^{X} -k_{x,\lambda}} \qquad (21)$$

Combining equations (19) and (21), the light attenuated by one cell of species j in a layer with a top depth of z, and bottom depth $z - M$, is given by:
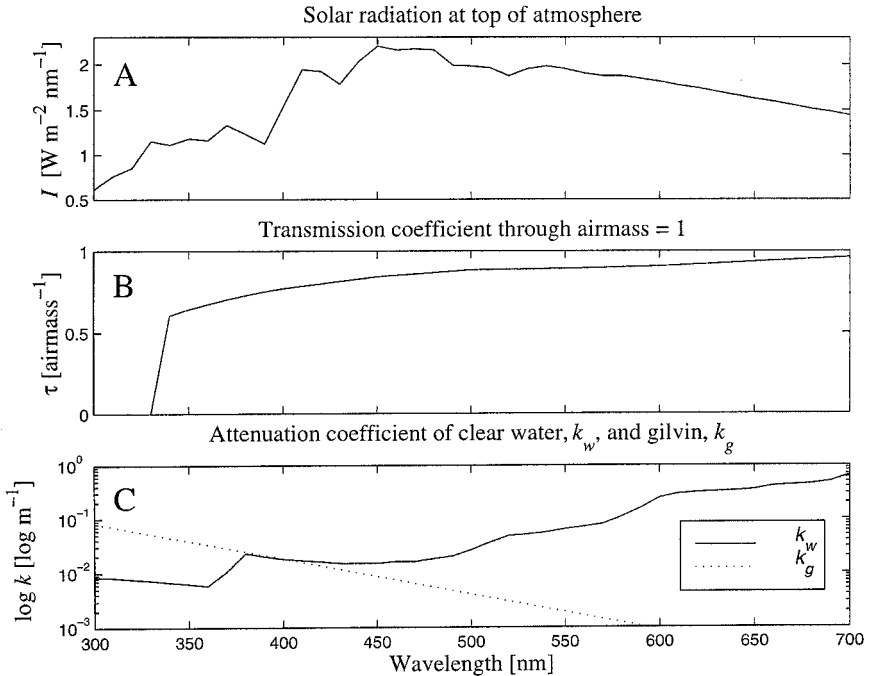

Fig. 3. Spectrally resolved optical properties of the atmosphere and water. (**A**) Solar radiation at the top of the atmosphere, I [W m^{-2} nm^{-1} = 8.3525 × 10^{-9} λ mol (photons) s^{-1} m^{-2} nm^{-1}] (Koller, 1965). (**B**) Transmission coefficient, τ (airmass^{-1}), of a cloudless atmosphere, zenith sun (airmass = 1) (Koller, 1965). (**C**) Attenuation coefficient of (—) clear water, k_w (m^{-1}) and (· · ·) gilvin (humic substances), k_g (m^{-1}), at typical open-ocean concentrations. Spectrally resolved k_g has been calculated using $k_{g,\lambda} = k_{g,\lambda_0} \exp(-S(\lambda - \lambda_0))$ (Bricaud et al., 1981), based on values typical of open-ocean environments of $k_{g,440 \text{ nm}} = 0.01$ m^{-1}, $S = 0.015$ nm^{-1} (Kirk, 1994).

95

$$(I_{j,\lambda})_{light\ attenuated} = \frac{A_v\, P_j\, \overline{aA}_{j,\lambda}}{k_{w,\lambda} + k_{g,\lambda} + \sum_{j'=1}^{p} A_v\, P_{j'}\, \overline{aA}_{j',\lambda}} \frac{(I_{z,\lambda} - I_{z-M,\lambda})}{A_v\, P_j\, M} \tag{22}$$

Light scattering has the potential to change the trajectory and pathlength, $M_{path,\lambda}$, of each photon. The effect of scattering on the light field is a function of wavelength, angle of incidence into the layer, and the ratio of scattering co-efficients and absorption coefficients (Kirk, 1994). Monte Carlo techniques (Kirk, 1981) can be used to track a large number of individual photons, to determine the average effect of scattering on $M_{path,\lambda}$. It has been found (Kirk, 1984) that the average effect of scattering on the pathlength of a photon at wavelength λ, $M_{path,\lambda}$, can be approximated for a water body with a given ratio of the total scattering coefficient, $b_{T,\lambda}$ (m^{-1}), to total absorption coefficient, $a_{T,\lambda}$ (m^{-1}), by:

$$M_{path,\lambda} = (M\sec\theta)\sqrt{1 + G(\theta)\frac{b_{T,\lambda}}{a_{T,\lambda}}} \tag{23}$$

where

$$G(\theta) = g_1\cos\theta - g_2 \tag{24}$$

$$a_{T,\lambda} = k_{w,\lambda} + k_{g,\lambda} + \sum_{j=1}^{p} A_v\, P_j\, \overline{aA}_{j,\lambda} \tag{25}$$

$$b_{T,\lambda} = b_{w,\lambda} + \sum_{j=1}^{p} b_{j,\lambda} A_v C_{\text{Chl}\ a,j} V_j\, P_j \tag{26}$$

G, g_1 and g_2 are dimensionless scattering constants characteristic of a water body (Table VIII), $b_{w,\lambda}$ is the scattering coefficient of sea water and its non-phytoplankton constituents at wavelength λ (m^{-1}) (Table VIII), and $b_{j,\lambda}$ is the scattering coefficient of phytoplankton species j at wavelength λ [m^2 mg (Chl a)$^{-1}$] (Table IX), V_j is the volume of phytoplankton species j (m^3) (Table X) and $C_{\text{Chl}\ a,j}$ is the concentration of chlorophyll a in phytoplankton species j (mol m^{-3}).

Experiments (Figure 4) show that high levels of radiation reduce the efficiency of use of light attenuated by pigments. This has been heuristically modelled using a changing internal cell quota of energy, q_j, similar to that used for nutrients [equation (10)] such that:

$$I_{light\ captured} = I_{attenuated}\left(\frac{q_j^{max} - q_j}{q_j^{max}}\right) \tag{27}$$

where q_j^{max} is the maximum cell quota of photons. Considering all photons between 300 and 700 nm to be equivalent in photosynthetic reactions, the change in internal cell quota of energy of species j due to light capture is given by:

$$\left(\frac{dq_j}{dt}\right)_{light\ capture} = \sum_{\lambda=300}^{700} \frac{a\overline{A}_{j,\lambda}}{k_{w,\lambda} + k_{g,\lambda} + \sum_{j'=1}^{p} A_v P_{j'}\ \overline{aA}_{j',\lambda}}$$

$$\frac{(I_{z,\lambda} - I_{z-M,\lambda})}{M}\ \left(\frac{q_j^{max} - q_j}{q_j^{max}}\right) \tag{28}$$

Growth rate of photosynthetic cells

The growth rate of photosynthetic cells is modelled using methodology employed in the study of chemical kinetics. Describing chemical reaction dynamics mechanistically using quantum theory is a major new field (Clary, 1998), but is not developed enough to describe complex biochemical reactions. As a result, empirical chemical kinetics methodology must be used. The reproduction of phytoplankton of species j, P_j, is assumed to be fully described by a simple chemical reaction: the reactants are a phytoplankton cell (including the molecules and energy it took to
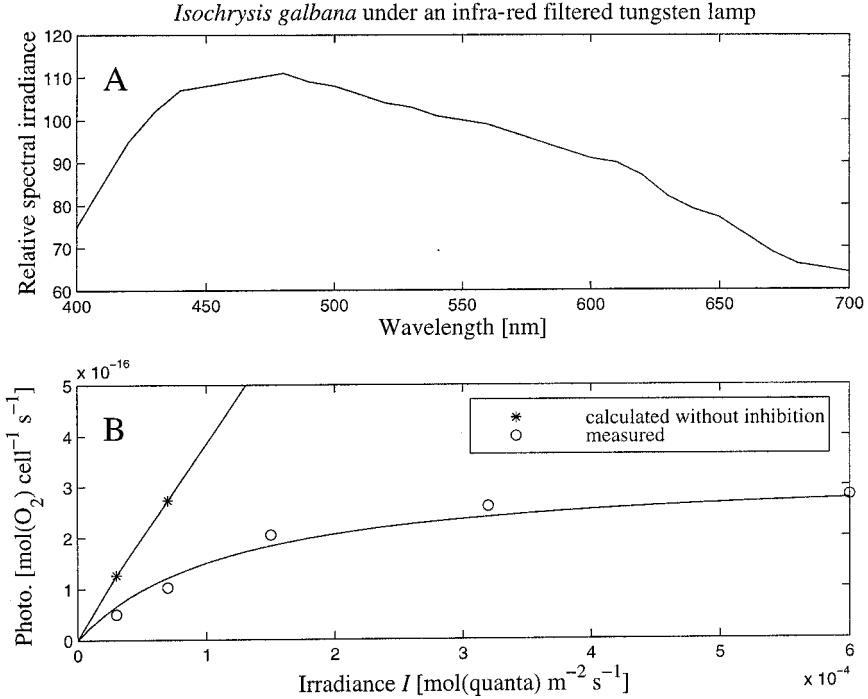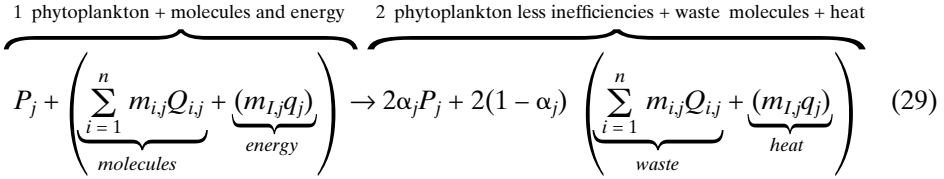

Fig. 4. Photosynthesis rate of *Isochrysis galbana* under an infra-red filtered tungsten lamp. (**A**) The relative spectral irradiance of a tungsten–iodine lamp with filter (Driscoll and Vaughan, 1978) between 400 and 700 nm. (**B**) (○) Measured photosynthesis rate and (∗) calculated based on uninhibited light capture in units of oxygen evolved for the prolate spheroid (aspect ratio = 1.84) *Isochrysis galbana* (Falkowski *et al.*, 1985). Calculated uninhibited light capture ($\overline{aA}\lambda$ $(I_\lambda)_{incident\ on\ j}$ [equation (17)] where $m_{O_2} = 10.4$, $\overline{aA}_{I.\ galbana}$ is calculated from formulae in Table IV using cell geometry in Table X, pigment ratios from Table IX, and absorbance according to equation (16)).

make it), and the molecules and energy required to make another phytoplankton cell; the products are two phytoplankton cells less inefficiencies, waste molecules and heat. The balanced chemical reaction becomes:

1 phytoplankton + molecules and energy   2 phytoplankton less inefficiencies + waste molecules + heat

$$P_j + \left(\sum_{i=1}^{n} m_{i,j}Q_{i,j} + \underbrace{(m_{I,j}q_j)}_{energy} \right) \rightarrow 2\alpha_j P_j + 2(1-\alpha_j) \left(\sum_{i=1}^{n} m_{i,j}Q_{i,j} + \underbrace{(m_{I,j}q_j)}_{heat} \right) \quad (29)$$

where $m_{i,j}$ is the stoichiometric coefficient for nutrient i, phytoplankton species j [mol $(Q_{i,j})$ mol $(P_j)^{-1}$], $m_{I,j}$ is the stoichiometric coefficient for energy, phytoplankton species j [mol (q_j) mol $(P_j)^{-1}$], and α_j is the efficiency of growth of phytoplankton species j (dimensionless). Equation (29) assumes that phytoplankton cells have a fixed stoichiometry, which could be, for example, the Redfield ratio (Table XIII). Under the rules of balancing chemical reactions, equation (29) can be used to describe population growth of sexually or asexually reproducing populations: the stoichiometry of equation (29) remains the same, but the growth rate of the population, k_j (defined below), will be seen to vary according to the parent to offspring ratio.

Based on equation (29), using chemical kinetic methodologies (Atkins, 1994), and assuming a first-order reaction rate of growth with respect to each reactant, the rates of change of P_j, $Q_{i,j}$ and q_j can be written as follows:

$$\frac{dP_j}{dt} = \alpha_j k_j q_j \left(\prod_{i=1}^{n} Q_{i,j} \right) P_j = \mu_j P_j \quad (30)$$

where k_j is the reaction rate constant [s^{-1} cell^{n+1} mol $(q)^{-1}$ $\Pi_{i=1}^{n}$ mol $(Q_i)^{-1}$] and μ_j is the growth rate of phytoplankton species j (s^{-1}). k_j can be determined at the maximum growth rate, μ_j^{max}, which is assumed to occur at an ideal temperature, with full internal quotas of nutrient and energy:

$$k_j = \frac{\mu_j^{max}}{\alpha_j q_j^{max} \, \Pi_{i=1}^{n} \, Q_{i,j}^{max}} \quad (31)$$

The rates of reaction of the different reactants can be equated:

$$\left(\frac{dP_j}{dt} \right)_{growth} = - \frac{A_v}{\alpha_j m_{i,j} P_j} \left(\frac{dQ_{i,j}}{dt} \right)_{growth} = - \frac{A_v}{\alpha_j m_{I,j} P_j} \left(\frac{dq_j}{dt} \right)_{growth} \quad (32)$$

so that:

$$\left(\frac{dQ_{i,j}}{dt} \right)_{growth} = - k_j \frac{m_{i,j}}{A_v} q_j \prod_{i'=1}^{n} Q_{i',j} \quad (33)$$

$$\left(\frac{\mathrm{d}q_j}{\mathrm{d}t}\right)_{growth} = -k_j \frac{m_{I,j}}{A_v} q_j \prod_{i'=1}^{n} Q_{i',j} \tag{34}$$

The inefficiency of phytoplankton growth results in a return of nutrients to the extracellular nutrient pool at the rate of:

$$\left(\frac{\mathrm{d}N_i}{\mathrm{d}t}\right)_{recycled} = \sum_{j=1}^{p} (1-\alpha_j)\, k_j m_{i,j} q_j \left(\prod_{i'=1}^{n} Q_{i,j}\right) P_j \tag{35}$$

The term 'recycled' has been used to distinguish the process in equation (35) from nutrient regeneration or remineralization, which are the breakdown of organic material (Libes, 1992). Recycled nutrient is better thought of as nutrient which has been taken into the cell, but then leaks or is excreted as a result of inefficiencies in the phytoplankton growth. This model includes no regeneration or remineralization.

Temperature dependence of growth rates

Temperature dependence of biochemical reactions is commonly fitted (Raven and Geider, 1988; Geider *et al.*, 1997) to the Arrhenius equation: an empirical formula based on an exponential change in reaction rate with temperature. The Arrhenius equation is given by (Atkins, 1994):

$$k = A e^{\frac{-E_a}{RT}} \tag{36}$$

where k is the reaction rate (s^{-1}), A is a constant (s^{-1}), E_a is the activation energy (J mol^{-1}), R is the universal gas constant = 8.31451 J K^{-1} mol^{-1} and T is temperature (K). Equation (36) is used to determine the growth rate constant at all temperatures, given the experimentally determined maximum growth rate at an ideal temperature, T_{ref}. The temperature dependence of k_j becomes:

$$k_j(T) = \frac{(\mu_j^{max})_{T_{ref,j}}}{\alpha_j q_j^{max} \prod_{i=1}^{n} Q_{i,j}^{max}} \exp\left[\frac{-E_{a,j}}{R}\left(\frac{1}{T} - \frac{1}{T_{ref,j}}\right)\right] \tag{37}$$

where $T_{ref,j}$ is the temperature at which the reaction rate constant, k_j, is at a maximum (K), and $E_{a,j}$ can be determined experimentally (Table XIII).

Sinking rates of plankton

A force balance on a particle in suspension determines the terminal vertical velocity, U_{sink} (m s^{-1}), of a cell due to a density difference between the fluid and the cell:

$$\underbrace{gV(\rho_{cell} - \rho_{water})}_{gravitational\ force} = \underbrace{C_D v U_{sink}}_{frictional\ force} \tag{38}$$

where g is the gravitational acceleration (m s^{-2}), V is the cell volume (m^3), ρ_{cell} and ρ_{water} are the density of the cell and surrounding water, respectively (kg m^{-3}), C_D is the drag coefficient (unitless), which is shape and orientation dependent (Table V), and v is the dynamic viscosity of water (kg m^{-1} s^{-1}). The removal rate of phytoplankton species j due to sinking from a well-mixed layer of thickness M (m) is given by:

$$\left(\frac{dP_j}{dt}\right)_{sinking} = -\frac{gV_j\,(\rho_j - \rho_{water})}{C_{D,j}vM}\,P_j \tag{39}$$

A similar force balance could be used to determine the sinking rate of herbivore species.

Plankton grazing

The process of a predator assimilating a prey can be divided into a series of events, such as searching, encounter, attack, capture and ingestion [for a review of the large body of work on these processes, see Dower *et al.* (1997)]. This paper considers only small herbivores, which are assumed to have no search or attack behaviours. Encounter occurs passively due to relative fluid motion between the predator and prey. Under this simplification, the grazing rate of a predator is dependent on its encounter, capture and ingestion rates of the prey (Shimeta *et al.*, 1995). Assuming these three rates to be independent, the grazing rate is determined by the slowest of encounter, capture and ingestion rates. Without sufficient theoretical understanding of plankton capture mechanisms, capture rates are assumed unlimiting [although Shimeta *et al.* (1995) suggest that capture may become limiting under high shear]. Plankton grazing rates therefore become the minimum of the encounter rate (a function of shear, swimming and sinking velocities) and the species-specific ingestion rate.

Encounter rates. Two different approaches have been used to estimate the encounter rate of particles. The first involves considering the velocities of all

Table V. Drag coefficients, C_D (dimensionless), of various shapes and orientation (Clift *et al.*, 1978). C_D is used to calculate terminal sinking velocity of cells [equation (38)] and Sherwood numbers in a uniform flow (Table III). r_a = aspect ratio = axial dimension/normal dimension; $r_{1,2}$ = orthogonal radii (m) where $r_1 > r_2$

Shape	Random	Axial	Normal
Sphere	$6\pi r_1$	$6\pi r_1$	$6\pi r_1$
Oblate spheroid	$\dfrac{6\pi r_1 \sqrt{1 - r_a^2}}{\cos^{-1} r_a}$	$\dfrac{8\pi r_1\,(1 - r_a^2)}{\frac{(1 - 2r_a^2)\cos^{-1} r_a}{\sqrt{1 - r_a^2}} + r_a}$	$\dfrac{16\pi r_1\,(1 - r_a^2)}{\frac{(3 - 2r_a^2)\cos^{-1} r_a}{\sqrt{1 - r_a^2}} - r_a}$
Prolate spheroid	$\dfrac{6\pi r_2 \sqrt{r_a^2 - 1}}{\ln\left(r_a + \sqrt{r_a^2 - 1}\right)}$	$\dfrac{8\pi r_2\,(r_a^2 - 1)}{\frac{(2r_a^2 - 1)\ln\left(r_a + \sqrt{r_a^2 - 1}\right)}{\sqrt{r_a^2 - 1}} - r_a}$	$\dfrac{16\pi r_2\,(r_a^2 - 1)}{\frac{(2r_a^2 - 3)\ln\left(r_a + \sqrt{r_a^2 - 1}\right)}{\sqrt{r_a^2 - 1}} + r_a}$

possible sources of relative motion between particles (swimming, sinking, turbulent motion, diffusion, feeding currents, etc.), to calculate an approximate relative velocity between particles, on which an encounter rate can be calculated (Gerritsen and Strickler, 1977; Rothschild and Osborn, 1988). An alternative approach, called coagulation theory (Jackson, 1995), calculates the encounter rate as the sum of encounter rates due to each source of relative motion. We have chosen to sum the relative velocities due to sinking and swimming of both predator and prey (Gerritsen and Strickler, 1977) to determine an encounter rate due to sinking and swimming, which is then added to the encounter rates calculated due to diffusion and turbulent motions following coagulation theory.

To calculate the relative velocity of the predator species k, and prey species j, due to their respective sinking and swimming velocities, $U_{j,k}$ (m s^{-1}), firstly their differential sinking (which is always along the vertical) rate is determined:

$$U_{sink,j,k} = U_{sink,j} - U_{sink,k} \tag{40}$$

The relative swimming velocity (addition of random swimming velocities of the predator and prey) is given by (Gerritsen and Strickler, 1977):

$$U_{swim,j,k} = \frac{U_{slow}^2 + 3U_{fast}^2}{3U_{fast}} \quad \text{where} \quad \begin{array}{l} U_{slow} = \min\left[U_{swim,j}, U_{swim,k}\right] \\[8pt] U_{fast} = \max\left[U_{swim,j}, U_{swim,k}\right] \end{array} \tag{41}$$

Assuming that the relative swimming direction of predator and prey is random, the relative velocity due to sinking and swimming, $U_{j,k}$ (m s^{-1}), is given by:

$$U_{j,k} = \frac{U_{slow}^2 + 3U_{fast}^2}{3U_{fast}} \quad \text{where} \quad \begin{array}{l} U_{slow} = \min\left[U_{swim,j,k}, U_{sink,j,k}\right] \\[8pt] U_{fast} = \max\left[U_{swim,j,k}, U_{sink,j,k}\right] \end{array} \tag{42}$$

Coagulation theory. Coagulation theory predicts that the encounter rate of a particle, say a predator, with other particles in a fluid, say the prey, P_j, can be given by:

$$\text{Encounter rate} = \phi_{j,k}P_j \tag{43}$$

where $\phi_{j,k}$ is the encounter rate coefficient (m^3 s^{-1}) and P_j is the concentration of prey species j (mol m^{-3}). $\phi_{j,k}$ is determined for encounter rates as a result of diffusion, relative velocity [$U_{j,k}$ from equation (42)] and turbulent shear (Table VI) using (Jackson, 1995):

$$\phi_{j,k} = \phi_{j,k,diffusion} + \phi_{j,k,relative\ velocity} + \phi_{j,k,turbulent\ shear} \tag{44}$$

When calculating the encounter rate coefficient for relative velocity and turbulent shear, two types of solutions are used:

Rectilinear solution—assumes that the presence of a larger organism does not change the velocity of smaller organisms. Filter-feeder contact rates are solved this way.

Curvilinear solution—assumes that smaller organisms follow streamlines around larger organisms, the two organisms only coming into contact if the streamline the smaller organism follows is within one smaller organism's radius of the larger organism. The most basic heterotrophs are solved this way.

At present, the rectilinear and curvilinear solutions of the encounter rate coefficient are only available for spherical cells (Table VI). To obtain the encounter rate coefficient for non-spherical shapes, an average spherical radius is assumed for the predator and prey when using the rectilinear solution, and the predator for the curvilinear solution. To account for the rotation due to shear of the prey as it passes around the predator, the prey's largest radius is used for the curvilinear solution.

To obtain the encounter rate for a population of H_k cells with a population of P_j cells, equation (43) becomes:

$$\text{Encounter rate} = A_v \phi_{j,k} P_j H_k \qquad (45)$$

where the Avogadro constant, A_v, is required to retain units of mol m^{-3} s^{-1}.
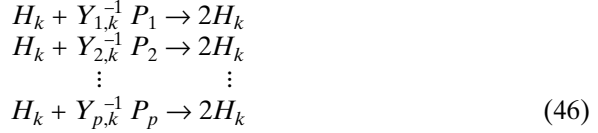
Ingestion rates. Herbivore maximum ingestion rates are reported (Hansen *et al.*, 1997), or can be calculated, given a maximum growth rate at unlimiting prey density, μ_k^{max}, and the yield of predator cells per prey, $Y_{j,k}$ (Eccleston-Parry and Leadbeater, 1994). The maximum ingestion rate of prey is then given by $\mu_k^{max} Y_{j,k}^{-1}$.

Table VI. Encounter rate coefficients for spherical cells. $\phi_{1,2}$ = encounter rate coefficient (m^3 s^{-1}) of two spheres, radii r_1 and r_2 where $r_2 > r_1$ (m). Rectilinear formulae assume the path of the cells is uninterrupted by the presence of other cells. Curvilinear formulae correct for the influence of large cells on the path of smaller cells. $p = r_1/r_2$; Boltzmann constant, $k_B = 1.38066 \times 10^{-23}$ J K^{-1}; T = temperature (K); μ = dynamic viscosity (kg s^{-1} m^{-1}); ϵ = mean rate of dissipation of turbulent kinetic energy (m^2 s^{-3}); and v = kinematic viscosity (m^2 s^{-1}) (Jackson, 1995)

Mechanism	Rectilinear encounter rate coefficient ϕ_r (m^3 s^{-1})	Curvilinear encounter rate coefficient ϕ_c (m^3 s^{-1})
Diffusion	$\dfrac{2k_BT}{3\mu}\left(\dfrac{1}{r_1}+\dfrac{1}{r_2}\right)(r_1+r_2)$	$\dfrac{2k_BT}{3\mu}\left(\dfrac{1}{r_1}+\dfrac{1}{r_2}\right)(r_1+r_2)$
Relative velocity	$\pi(r_1+r_2)^2 U_{1,2}$	$0.5\pi r_1^2 U_{1,2}$
Turbulent shear	$1.3\left(\dfrac{\epsilon}{v}\right)^{0.5}(r_1+r_2)^3$	$9.8\dfrac{p^2}{(1+2p)^2}\left(\dfrac{\epsilon}{v}\right)^{0.5}(r_1+r_2)^3$

Growth rate of herbivore cells

Herbivore growth rate is a function of temperature, the encounter rate of phytoplankton and herbivore cells, and the maximum herbivore ingestion rate of phytoplankton. It is assumed that the growth of herbivore species k can be described by a series of chemical reactions, one for the assimilation of each prey species P_j, $j = 1, \ldots, p$ such that:

$$
\begin{aligned}
H_k + Y_{1,k}^{-1} P_1 &\rightarrow 2H_k \\
H_k + Y_{2,k}^{-1} P_2 &\rightarrow 2H_k \\
\vdots \qquad & \qquad \vdots \\
H_k + Y_{p,k}^{-1} P_p &\rightarrow 2H_k
\end{aligned}
\tag{46}
$$

Like equation (29), equation (46) is a balanced chemical reaction, describing sexually or asexually reproducing populations of variable parent to offspring ratios. Herbivore growth rate in unlimiting prey concentrations is assumed to be exponential. The change in herbivore species k with time due to grazing on phytoplankton species $j = 1, \ldots, p$ is assumed to be proportional to the minimum of the prey-saturated growth rate, μ_k^{max} (s^{-1}), and the product of the encounter rate per predator, $A_v \sum_{j=1}^{p} \phi_{j,k} P_j$, and the yield of predator per prey, $Y_{j,k}$:

$$
\left(\frac{dH_k}{dt} \right)_{grazing\ uptake} = \min \left[\mu_k^{max}, \ A_v \sum_{j=1}^{p} \phi_{j,k} P_j Y_{j,k} \right] H_k
\tag{47}
$$

If predator k is not ingestion rate limited, the resultant grazing loss in phytoplankton species j is given by:

$$
\left(\frac{dP_j}{dt} \right)_{grazing\ loss\ to\ H_k} = A_v \phi_{j,k} P_j H_k
\tag{48}
$$

If a predator k is ingestion rate limited, all phytoplankton grazing loss terms of k will be a function of the population of the predator, and the predator preference for each prey species. Assuming that the predator k has an equal preference for all prey, the grazing loss of phytoplankton species j becomes a function of the population of the predator k, and the fraction of encounters of species j with k in a diet of $1, \ldots, j'$. Therefore, the loss term for population P_j in a diet of $P_{j'}$, $j' = 1, \ldots, p$, for ingestion rate-limited predator k with no prey preference is given by:

$$
\left(\frac{dP_j}{dt} \right)_{grazing\ loss\ to\ H_k} = \frac{\phi_{j,k} P_j}{\sum_{j'=1}^{p} \phi_{j',k} P_{j'}} \ \mu_k^{max} Y_{j,k}^{-1} H_k
\tag{49}
$$

Combining equations (48) and (49), the grazing loss term of phytoplankton species j in an assemblage of $j' = 1, \ldots, p$ to grazers H_k, $k = 1, \ldots, h$ is given by:

$$\left(\frac{\mathrm{d}P_j}{\mathrm{d}t}\right)_{grazing} = \sum_{k=1}^{h} \begin{cases} -A_v \phi_{j,k} P_j H_k & \text{if } A_v \sum_{j'=1}^{p} \phi_{j',k} P_{j'} Y_{j',k} < \mu_k^{max} \\[3mm] -\dfrac{\phi_{j,k} P_j}{\sum_{j'=1}^{p} \phi_{j',k} P_{j'}} \mu_k^{max} Y_{j,k}^{-1} H_k & \text{if } \mu_k^{max} < A_v \sum_{j'=1}^{p} \phi_{j',k} P_{j'} Y_{j',k} \end{cases} \tag{50}$$

Equation (50) implies that the grazing loss to an ingestion rate-limited predator is less than the loss to an encounter rate-limited predator for the same prey species concentration. For two competing prey species, P_1 and P_2, the bloom of species P_1, if it results in the ingestion limitation of a common predator, will reduce the grazing pressure on P_2.

The temperature dependence of herbivore growth rates can be fitted to the Arrhenius equation [equation (36)] in a similar manner to phytoplankton [equation (37)]:

$$\mu_k^{max}(T) = (\mu_k^{max})_{T_{ref,k}} \exp\left[\frac{-E_{a,k}}{R}\left(\frac{1}{T} - \frac{1}{T_{ref,k}}\right)\right] \tag{51}$$

where $T_{ref,k}$ is the temperature at which the prey-saturated growth rate, μ_k^{max}, is a maximum (K); $E_{a,k}$ can be determined experimentally (Table XIV); yield, $Y_{j,k}$, is assumed to be unaffected by temperature, and the encounter rate coefficient, $\phi_{j,k}$, is a known function of temperature (Table VI).

Mixing

In addition to the interactions described by the ODEs above, plankton populations are also affected by fluid mixing, which is best described using partial differential equations (PDEs). Mixing of scalars such as nutrient, salinity and cells, here simplified to mixing in the vertical (z) direction only, takes the form (Sharples and Tett, 1994):

$$\frac{\partial S_z}{\partial t} = \frac{\partial}{\partial z}\left(K_z \frac{\partial S_z}{\partial z}\right) + \left(\frac{dS_z}{dt}\right)_{\text{loss and gain at depth } z} \tag{52}$$

where S_z is the value of scalar S at depth z and K_z is the vertical coefficient of eddy diffusivity (m² s⁻¹). The mixing rate of the properties of a cell, such as internal nutrient quota, Q, is given by:

$$\frac{\partial Q_z}{\partial t} = \left(\frac{\partial}{\partial z}\left(\frac{K_z}{P_z}\frac{\partial(P_z Q_z)}{\partial z}\right)\right) + \left(\frac{dQ_z}{dt}\right)_{\text{loss and gain at depth } z} \tag{53}$$

To integrate PDEs forward in time, a variety of differencing schemes can be used. To illustrate the mixing of the properties of a cell, the forward-time centred-space (FTCS) (Hoffman, 1992) differencing scheme is used:

$$P_i^{n+1} = P_i^n + K_z \left(P_{i+1}^n - 2P_i^n + P_{i-1}^n \right) \qquad (54)$$

where P_i^n represents the phytoplankton cell numbers at time n, position i. The mixing for internal properties becomes:

$$P_i^{n+1} Q_i^{n+1} = P_i^n Q_i^n + K_z \left(\overbrace{+ P_{i+1}^n Q_{i+1}^n}^{\text{nutrient from above}} \underbrace{- 2P_i^n Q_i^n}_{\text{lost to above and below}} \overbrace{+ P_{i-1}^n Q_{i-1}^n}^{\text{nutrient from below}} \right) \qquad (55)$$

It should be noted that in equation (53), and its numerical approximation equation (55), the direction of the flux of internal nutrient quota, Q, is dependent on the gradient in Q only, but the magnitude is a function of the gradient of both P and Q, as would be expected.

Instead of tracking individual molecules and their internal physiological states (Lagrangian formulation), equation (55) mixes the average internal properties (Eulerian formulation). Errors resulting from using a Eulerian approximation (of, at the scale of the plankton, the Lagrangian reality) should be small if, for an individual, the time to move between layers is large compared to the time to reach the average value of the layer from gains and losses at that depth. A comparison between Lagrangian and Eulerian models of phytoplankton growth found only a small (20%) difference in phytoplankton growth (McGillicuddy, 1995).

The model equations

Including the effects of mixing, the model equations are given in Table VII. The equations contain n nutrient species, p phytoplankton species and h herbivore species. Phytoplankton species are differentiated on the basis of pigment assemblages (Table IX) and shape (Table X). Herbivores are differentiated by shape, swimming velocity, feeding mechanism (Table XII) and yield of prey per herbivore (Table XI). Other biological parameters required, but not routinely measured in laboratory experiments, include the ability to store nutrients, cell stoichiometry, maximum growth rate, density, swimming velocity and growth efficiency of phytoplankton, and the density of zooplankton. These values have been obtained from general size-dependent relationships found in the literature (Tables XIII and XIV).

Experimental validation of functional forms

Published laboratory experiments involving plankton populations can be used to assess the performance of the presented mechanistic functional forms, based on individual plankton cells, to describe population dynamics.

Nutrient uptake. Equation (14) is a function of extracellular nutrient concentration, fluid motion, phytoplankton shape, internal cell quota (or physiological state), and the saturation and maximum activity of internal uptake processes. No published experimental studies have investigated all of these variables. However,

Table VII. The model equations. Units for state variables are: N_i [mol (N_i) m^{-3}]; $Q_{i,j}$ [mol (Q_i) cell $(P_j)^{-1}$]; q_j [mol (q) cell $(P_j)^{-1}$]; P_j [mol (P_j) m^{-3}]; H_k [mol (H_k) m^{-3}]

$$\frac{\partial N_i}{\partial t} = \underbrace{\frac{\partial}{\partial t}\left(K_z \frac{\partial N_i}{\partial z}\right)}_{mixing} - \underbrace{\sum_{j=1}^{p} \psi_j D_i N_i P_j A_v Sh_{i,j}\left(\frac{Q_{i,j}^{max}-Q_{i,j}}{Q_{i,j}^{max}}\right)}_{uptake\ by\ phytoplankton} + \underbrace{\sum_{j=1}^{p}(1-\alpha_j)k_j m_{i,j}q_j\left(\prod_{i'=1}^{n} Q_{i',j}\right)P_j}_{recycled}$$

$$\frac{\partial Q_{i,j}}{\partial t} = \underbrace{\left(\frac{\partial}{\partial t}\left(\frac{K_z}{P_j}\frac{\partial(Q_{i,j}P_j)}{\partial z}\right)\right)}_{mixing} + \underbrace{\psi_j D_i N_i Sh_{ij}\left(\frac{Q_{i,j}^{max}-Q_{i,j}}{Q_{i,j}^{max}}\right)}_{uptake} - \underbrace{k_j \frac{m_{i,j}}{A_v}q_j\prod_{i'=1}^{n} Q_{i',j}}_{consumption\ for\ growth}$$

$$\frac{\partial q_j}{\partial t} = \underbrace{\left(\frac{\partial}{\partial t}\left(\frac{K_z}{P_j}\frac{\partial(q_j P_j)}{\partial z}\right)\right)}_{mixing} - \underbrace{k_j \frac{m_{I,j}}{A_v}q_j\prod_{i=1}^{n} Q_{i,j}}_{consumption\ for\ growth}$$

$$+ \underbrace{\frac{a\overline{A}_{j,\lambda}}{k_{w,\lambda}+k_{g,\lambda}+\sum_{j'=1}^{p} A_v P_{j'}a\overline{A}_{j',\lambda}}\frac{(I_{z-M,\lambda}-I_{z,\lambda})}{M}\left(\frac{q_j^{max}-q_j}{q_j^{max}}\right)}_{light\ captured\ and\ stored}$$

$$\frac{\partial P_j}{\partial t} = \underbrace{\frac{\partial}{\partial t}\left(K_z \frac{\partial P_j}{\partial z}\right)}_{mixing} + \underbrace{\alpha_j k_j P_j q_j\prod_{i=1}^{n} Q_{i,j}}_{growth} - \underbrace{\frac{gV_j(\rho_j-\rho_{water})}{C_{D,j}vM}P_j}_{sinking}$$

$$-\sum_{k=1}^{h}\begin{cases} A_v\phi_{j,k}P_j H_k & \text{if } A_v\sum_{j'=1}^{p}\phi_{j',k}P_{j'}Y_{j',k} < \mu_k^{max} \\ \dfrac{\phi_{j,k}P_j}{\sum_{j'=1}^{p}\phi_{j',k}P_{j'}}\mu_k^{max}Y_{j,k}^{-1}H_k & \text{if } \mu_k^{max} < A_v\sum_{j'=1}^{p}\phi_{j',k}P_{j'}Y_{j',k} \end{cases}$$

$$\underbrace{\phantom{-\sum_{k=1}^{h}\begin{cases} A_v\phi_{j,k}P_j H_k \end{cases}}}_{grazing\ loss}$$

$$\frac{\partial H_k}{\partial t} = \underbrace{\frac{\partial}{\partial t}\left(K_z \frac{\partial H_k}{\partial z}\right)}_{mixing} + \underbrace{\min\left[\mu_k^{max}, A_v\sum_{j=1}^{p}\phi_{j,k}P_j Y_{j,k}\right]H_k}_{grazing\ uptake}$$

experiments on populations of a single species of cyanobacterium (Mierle, 1985a), a diatom (Pasciak and Gavis, 1975) and a macroalga (Smith and Walker, 1980) have been conducted to test the validity of the Hill–Whittington equation (Hill and Whittingham, 1955):

$$\frac{J^2}{\psi DSh} - \left(K + C_b + \frac{V}{\psi DSh}\right)J + VC_b = 0 \tag{56}$$

The functional form for nutrient uptake proposed earlier, equation (14), is based on equation (56), with the addition of the heuristically determined function for enzyme activity, K, on the internal cell processes [equation (12)]. Using parameter values for a cyanobacterium (Figure 5) and a diatom (Figure 6), the approximation of equation (14) given earlier, equation (15), is found to be good ($\pm 50\%$) in all regions except those where there is both high C_b and low Q (Figures 5 and 6). However, conditions of both high C_b and low Q are unlikely to be present in natural environments, or numerical models of phytoplankton growth. Furthermore, equation (15) has a dependence on internal cell quota, Q, similar to that used by other authors (Sharples and Tett, 1994), and does not require determination of V, or K_o, which is problematic (see above).

Light capture. Figure 7 compares the measured spectrally resolved Chl *a*-specific absorbance of pigments extracted from two species of cyanobacteria with the
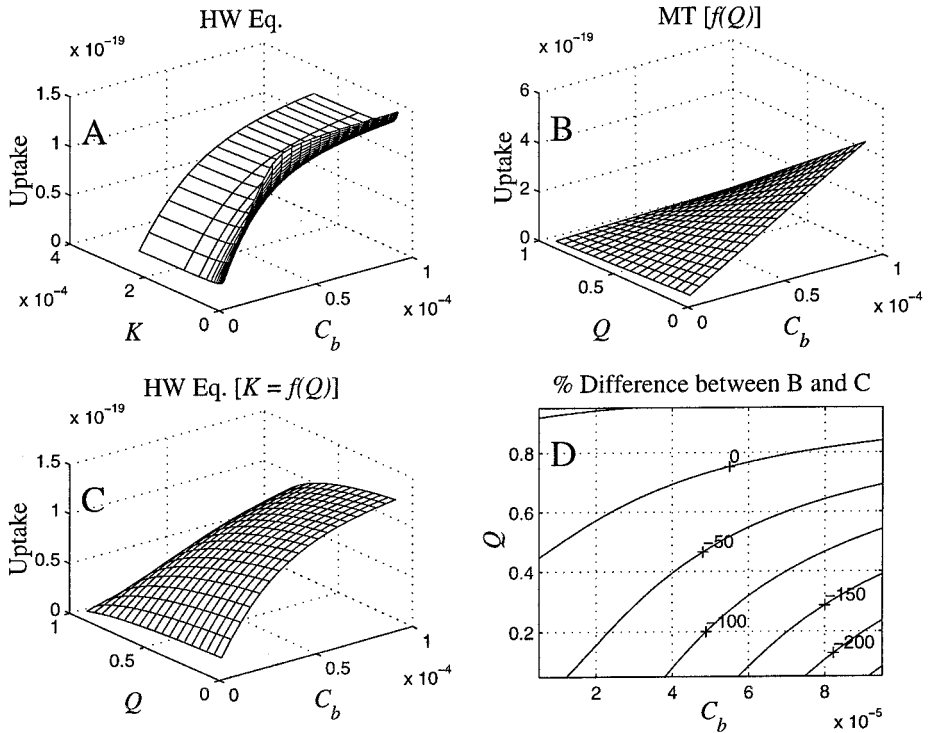

Fig. 5. Analysis of nutrient uptake functional forms [equations (14) and (15)] using parameters (K, V) determined from laboratory experiments of phosphate uptake rates to the cyanobacterium *Synechococcus leopoliensis* (Mierle, 1985b), as a function of extracellular concentration and internal cell quota of nitrate. (**A**) Uptake determined using the Hill–Whittingham equation (HW) [equation (56)]. (**B**) Uptake determined using mass transfer (MT) formulation dependent on internal cell quotient, Q [equation (15)]. (**C**) Uptake determined using HW, with K a function of Q (HW equation [$K = f(Q)$]) [equation (14)]. (**D**) Percentage difference between (B) and (C). (HW equation [$K = f(Q)$]) is the most theoretically justifiable functional form, but MT has been preferred because of a lack of experimental determinations of K_o and V.
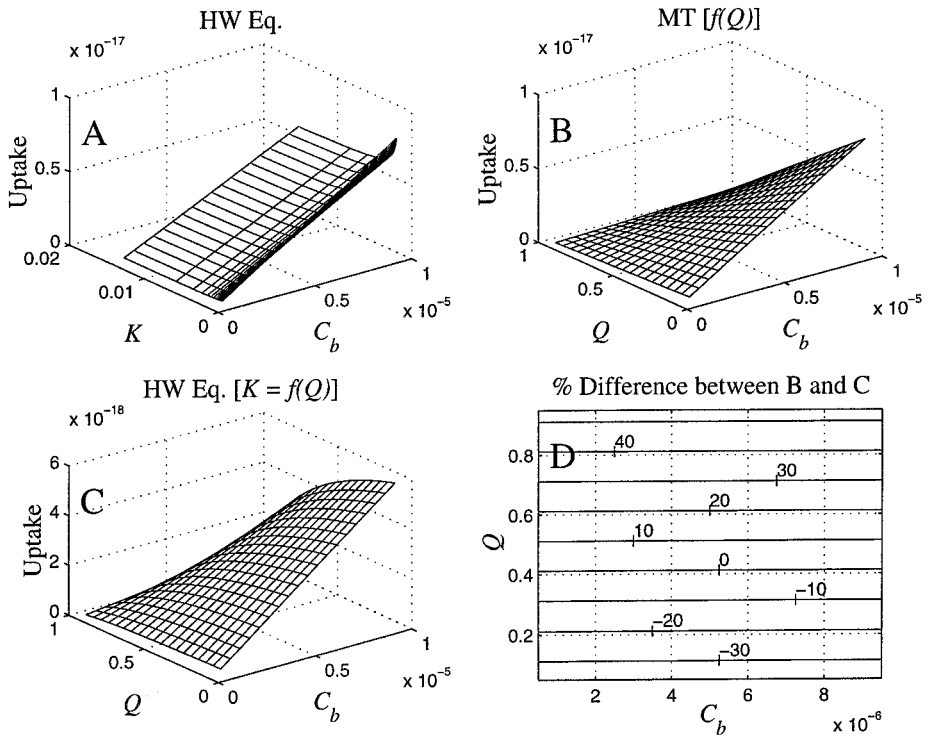
Fig. 6. Analysis of nutrient uptake functional forms [equations (14) and (15)] using parameters (K, V) determined from laboratory experiments of nitrate uptake to the diatom *Dictylum brightwelli* (Pasciak and Gavis, 1975), as a function of extracellular concentration and internal cell quota of nitrate. See Figure 5.

calculated value, assuming the pigment assemblage is made up of Chl *a*, Chl *b*, Chl *c* and carotenoids (Table IX) with absorbances described by Gaussian curves [equation (16)]. Errors are a result of using only four pigment types, and the lack of fit of the true pigment absorbances to Gaussian curves. These errors could be avoided by using measured spectrally resolved absorbances.

The equations used to determine $\overline{aA}$ (Table IV) are exact for particular shapes with evenly distributed pigment, but are only as good as the approximation of the phytoplankton shape. The initial slope of a photosynthesis versus irradiance curve should be approximated by $\overline{aA}\,m_{O_2}$, where $m_{O_2} = 10.4$. Figure 4 compares measured values of *Isochrysis galbana* with those calculated using cell geometry in Table X, pigment ratios from Table IX, and absorbance according to equation (16).

Grazing rates. The ingestion rate of six protozoan species has been investigated in a stagnant fluid (swimming only) and in shear flows (Shimeta *et al.*, 1995). In a stagnant fluid, coagulation theory satisfactorily predicted the slope of ingestion rate versus prey concentration (Figure 8) for a number of protozoan species. The
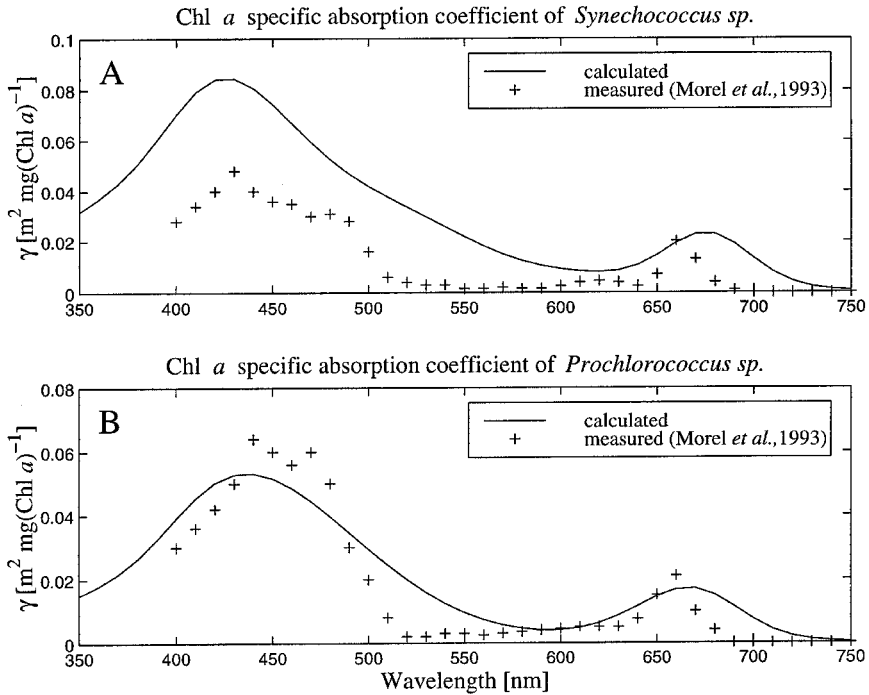
Chl a specific absorption coefficient of *Synechococcus sp.*

Chl a specific absorption coefficient of *Prochlorococcus sp.*

Fig. 7. (+) Measured and (–) calculated Chl a-specific absorbance [m^2 mg (Chl $a)^{-1}$] based on absorption coefficients calculated using equation (16), W_ξ, λ_ξ and γ_ξ from Hoepffner and Sathyendranath (1991), and pigment concentrations, C_ξ, from Table IX of *Synechococcus* sp. and *Prochlorococcus* sp.

growth kinetics of six heterotrophic flagellates has been studied under stagnant conditions, at higher prey concentration (Eccleston-Parry and Leadbeater, 1994). Although the encounter rate coefficient still predicted the initial slope of the growth rate versus prey concentration curve, a deviation from this line was observed for *Codosiga gracilis* before ingestion rate limitation is reached (Figure 9). This may be explained by a reduced swimming velocity at higher prey concentrations, although such an effect was not included in the model as presented.

Sinking rates. The force balance for particle sinking, equation (38), is well known (Atkins, 1994). Measurement of sedimentation rates in the open ocean suggests that equation (38) underestimates the sinking velocities for small phytoplankton cells (radius < 5 μm) by 1–3 orders of magnitude (Kennett, 1982). For a long time, this anomaly of increased sedimentation rates has been explained by the formation of aggregates (Lohmann, 1902). The understanding of the mechanisms of aggregation formation, or coagulation, has been well studied at the individual scale (Jackson, 1995). However, due to increasing the simulation time, coagulation will not be included in the presented model. In open-ocean environments, where plankton are dilute, growth, grazing and mixing are probably more important terms than sinking, even including coagulation. In coastal regions, however,
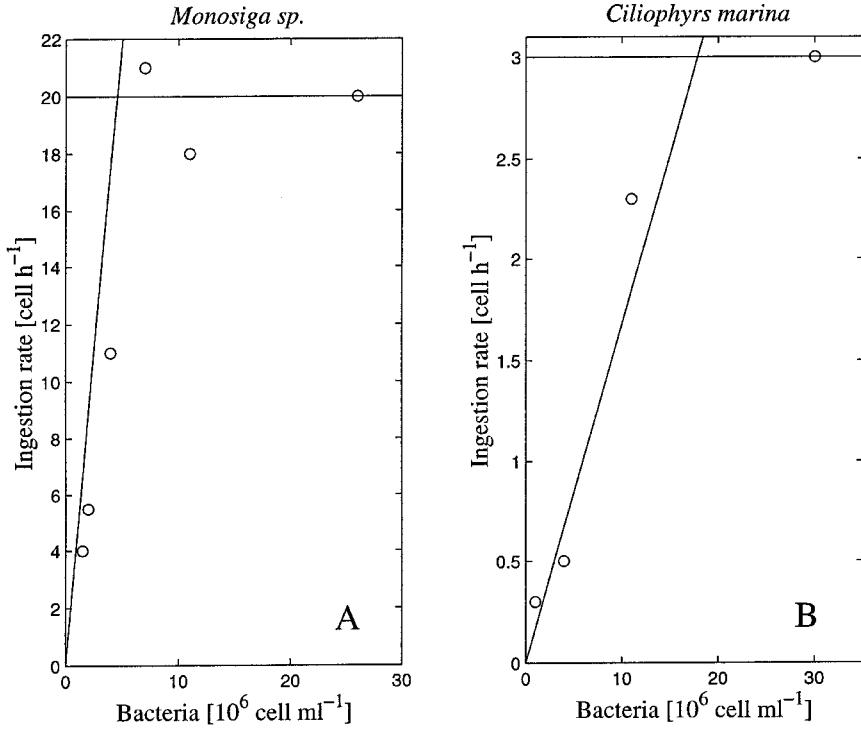
109

Fig. 8. ($\bigcirc$) Measured ingestion rate of *Monosiga* sp. and *Ciliophyrs marina* (Shimeta *et al.*, 1995) and (–) predicted ingestion rate using coagulation theory. For *Monosiga* sp.: dimensions $3 \times 3 \times 3$ μm, $U_{swim,pred} = 30$ μm s^{-1} and non-motile bacteria $0.6 \times 0.6 \times 0.6$ μm, $\epsilon = 0$ m^2 s^{-3}, rectilinear encounter rate coefficient $\phi = 4.4 \times 10^{-12}$ m^3 h^{-1}. For *C.marina*: dimensions $30 \times 30 \times 30$ μm, $U_{swim,pred} = 0$ μm s^{-1} and non-motile bacteria $2 \times 2 \times 2$ μm, $\epsilon = 0$ m^2 s^{-3}, encounter rate coefficient for diffusion, $\phi = 168 \times 10^{-15}$ m^3 h^{-1}. The horizontal line represents the ingestion rate limit used in Table XI.

coagulation can result in sinking becoming the dominant phytoplankton loss term, and has been used to explain the ending of phytoplankton blooms (Kiørboe *et al.*, 1996).

The chemical reaction of phytoplankton growth. The behaviour of the 'chemical reaction' describing phytoplankton growth [equation (29)] (CR) can be simplified at steady state, assuming only an internal quota for one nutrient, Q, and energy, q, to two simultaneous non-linear equations:

$$k_1 \frac{Q^{max} - Q}{Q^{max}} = m_Q k_3 Q q \tag{57}$$

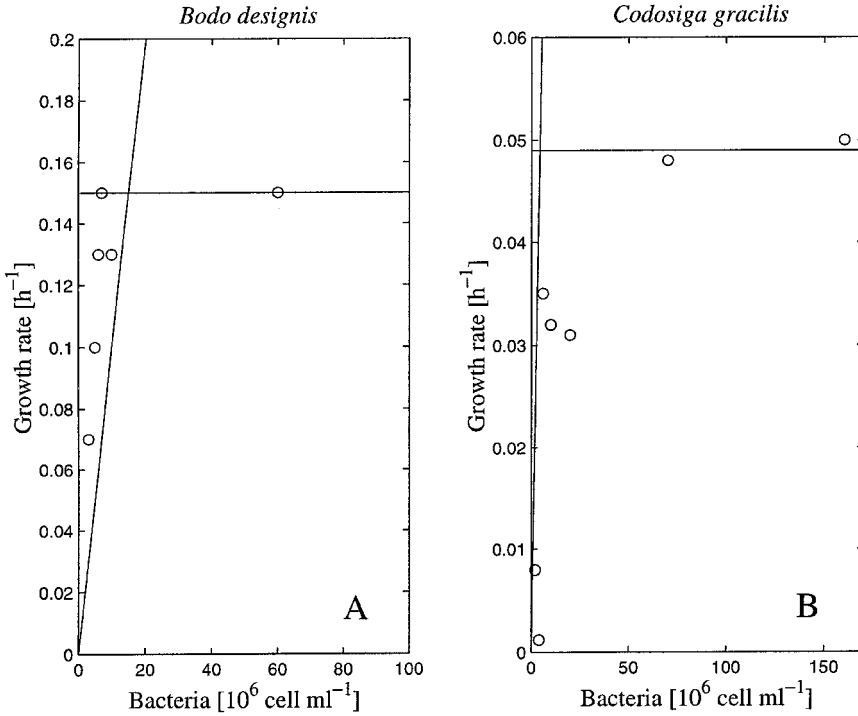$$k_2 \frac{q^{max} - q}{q^{max}} = m_q k_3 Q q \tag{58}$$

Fig. 9. (○) Measured growth rate of *Bodo designis* (Eccleston-Parry and Leadbeater, 1994) and (–) predicted growth rate using coagulation theory, and assuming exponential growth. For *B.designis*: dimensions $2.7 \times 2.7 \times 2.7$ μm, $U_{swim,pred} = 80$ μm s^{-1} and non-motile bacteria $1.5 \times 1.5 \times 1.5$ μm, $\epsilon = 0$ m^2 s^{-3}, rectilinear encounter rate coefficient $\phi = 16 \times 10^{-12}$, yield $\gamma = 1/693$ predator prey^{-1}. For *Codosiga gracilis*: dimensions $2.8 \times 2.8 \times 2.8$ μm, $U_{swim,pred} = 215$ μm s^{-1} and non-motile bacteria $1.5 \times 1.5 \times 1.5$ μm, $\epsilon = 0$ m^2 s^{-3}, rectilinear encounter rate coefficient $\phi = 45 \times 10^{-12}$ m^3 h^{-1}, yield $\gamma = 1/3990$ predator prey^{-1}. The horizontal line represents the ingestion rate limit used in Table XI.

where $k_1 = \psi DNSh$ [mol (Q) s^{-1}], $k_2 = \overline{aAl}$ [mol (q) s^{-1}] and $k_3 = k_j/A_v$ [mol s^{-1} mol (Q)$^{-1}$ mol (q)$^{-1}$] are, respectively, the nutrient uptake, light capture and growth rate constants for an individual cell. These equations have been solved for growth rate, k_3Qq, at $m_Q = m_q = 1$ (Figure 10). Numerical solutions were obtained using MATLAB software, by applying Newton's method for solving systems of non-linear equations, truncating the Taylor series approximation to one term, and using Gaussian elimination to solve the intermediate linear simultaneous equations, until successive approximations were within 10^{-9} (Hoffman, 1992).

The growth functional forms most commonly used in plankton population models are: (i) the multiplicative form (MP) (Steele and Henderson, 1981; Fasham *et al.*, 1990; Taylor and Stephens, 1993), which can be written as:

$$(\text{growth rate})_{MP} = k_1 k_2 k_3 \tag{59}$$

111

Growth rate constant, $k_3 = 1$ Growth rate constant, $k_3 = 4$

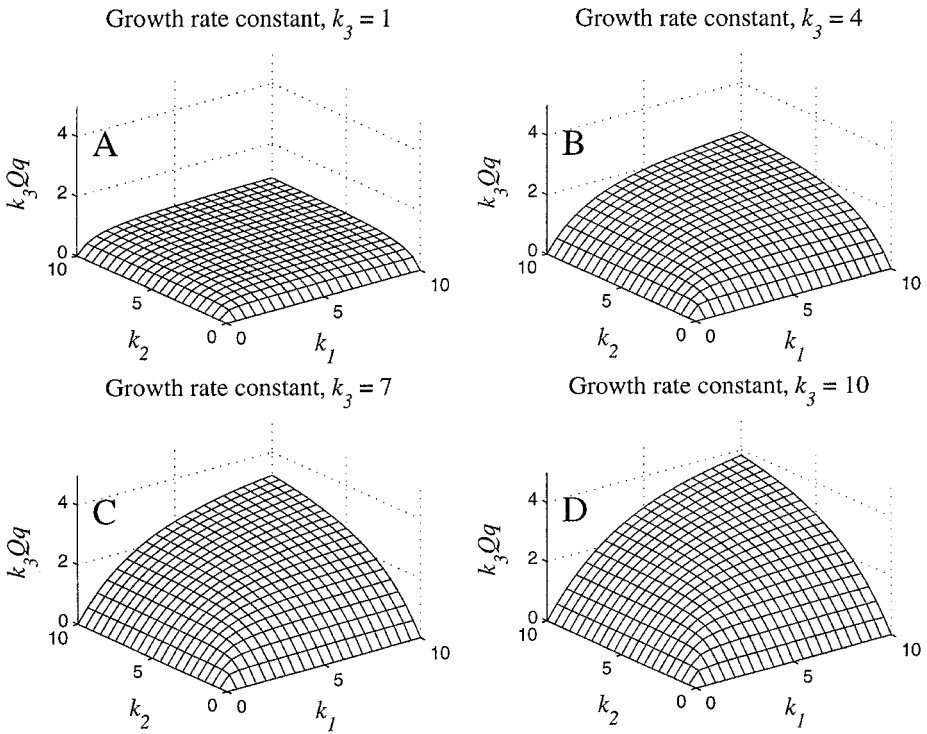Growth rate constant, $k_3 = 7$ Growth rate constant, $k_3 = 10$

Fig. 10. Steady-state analysis of non-linear simultaneous equations (57) and (58) using Newton's method for non-linear equations (Hoffman, 1992). (**A**) $k_3 = 1$; (**B**) $k_3 = 4$; (**C**) $k_3 = 7$; (**D**) $k_3 = 10$. In the limit of one rate (k_1, k_2 or k_3) being much smaller than the other two, the growth rate k_3Qq becomes proportional to the smallest rate only. This behaviour is similar to the 'Law of the Minimum' (von Liebig, 1840).

and (ii) the threshold or 'Law of the Minimum' form (LM) (de Baar, 1994), in which the growth rate is dependent on the slowest uptake rate and the growth rate constant:

$$(\text{growth rate})_{LM} = (\min\ [k_1, k_2]k_3) \qquad (60)$$

A comparison of the temperature dependence of growth rates obtained using CR, MP and LM functional forms has been made for a variety of values of k_1, k_2 and k_3 (Figure 11) based on the assumptions: k_1 is proportional to extracellular concentration and experiences a linear increase of 0.87 every 10 K (based on molecular diffusivity of nitrate), k_2 is proportional to irradiance, and k_3 doubles every 10 K.

The CR form was chosen because: (i) chemical kinetics methodology is used in many applications; (ii) the cell quotas Q and q take into account the light and nutrient histories of the cells; (iii) the non-linear characteristics of equations (57) and (58) fitted laboratory experiments with a minimum of parameters (i.e. it did not require the addition of half-saturation constants for nutrient and energy uptake); and (iv) the CR form fits observed temperature dependencies of algal
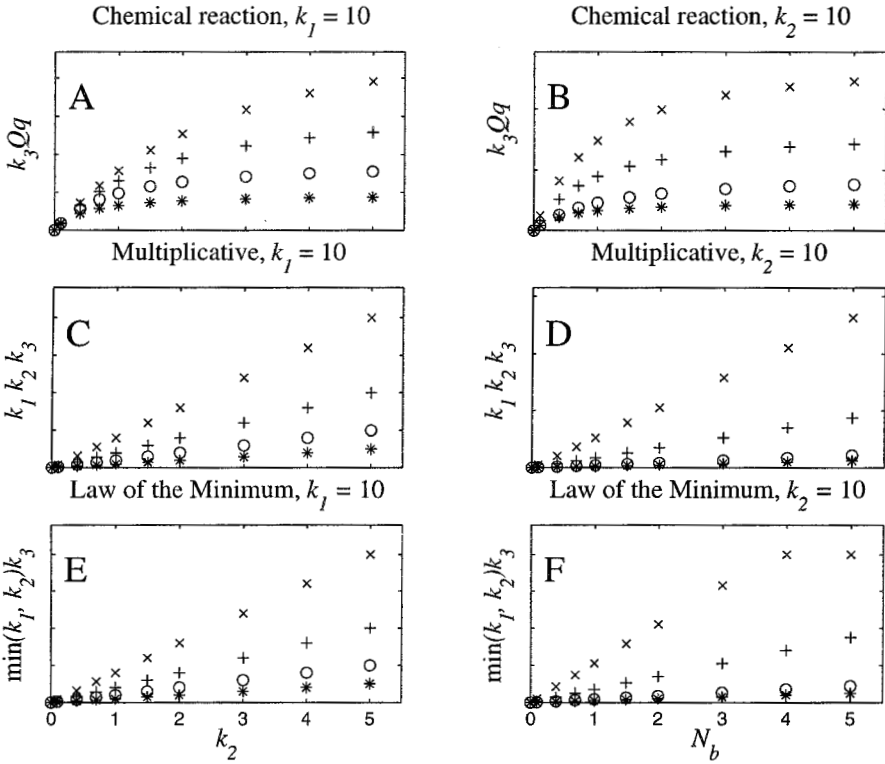
Fig. 11. A comparison of phytoplankton growth functional forms (CR, MP and LM) at four different temperatures in low-light (left column) and low-nutrient (right column) conditions. The four different temperatures, 10 K apart, correspond to a doubling of k_3, and are solved using: (∗) $k_3 = 0.5$; (○) $k_3 = 1$; (+) $k_3 = 2$; (×) $k_3 = 4$.

growth rate at low nutrient and low light conditions. For example, laboratory experiments at unlimiting nutrient concentrations ($k_1 = 10$) and low light conditions show that algal growth rate is independent of temperature (Kirk, 1994). This is also the case for the CR form (Figure 11A), but both the MP (Figure 11C) and LM (Figure 11E) forms are at least linear functions of temperature for all light conditions. At unlimiting light ($k_3 = 10$) and low nutrient conditions, nutrient uptake is a positive function of temperature (Raven and Geider, 1988), which the CR form also predicts (Figure 11B).

Mathematically, the CR form shares similar characteristics to both alternate functional forms. The CR growth term is a multiplicative form, albeit based on internal cell quotas rather than extracellular quantities, and for a nutrient with a much slower supply rate CR approximates the 'Law of the Minimum':

$$\frac{\dfrac{\partial(k_3 Qq)}{\partial k_1}}{\dfrac{\partial(k_3 Qq)}{\partial k_2}} \rightarrow \infty \text{ as } \frac{k_2}{k_1} \rightarrow \infty \text{ and } \frac{k_3}{k_1} \rightarrow \infty \qquad (61)$$

113

where the symmetry of equations (57) and (58) allows the interchanging of k_1 and k_2 in equation (61). Using the CR form satisfies the need for a dynamic balance of multiple growth and loss terms, with the observation in many natural environments of phytoplankton populations which are well approximated by the 'Law of the Minimum' (de Baar, 1994).

Model simulation

The model was run to simulate plankton population dynamics in the oceanic mixed layer at Bermuda Station 'S' (32º10′N, 65º30′W) and OWS 'India' (59ºN, 19ºW). Depth and seasonally changing mixing rates (K_z) were simplified to a seasonally varying mixed layer depth [determined using climatic monthly averages (Fasham *et al*., 1990)], and a fixed exchange rate, D_e (m s^{-1}), with the bottom water. Light was assumed to consist of 41 discrete wavelengths, at 10 nm intervals, from 300 to 700 nm. The spectrally resolved incoming solar radiation at the top of the atmosphere (Figure 3) was attenuated through the atmosphere by the sum of a spectrally resolved cloudless atmosphere transmission coefficient, τ (airmass^{-1}) (Figure 3), and an average attenuation rate characteristic of shortwave radiation through 4 otkas of cloud (Smith and Dobson, 1984). Azimuth angle is a function of latitude, day and hour (Brock, 1981), and is used to determine the intensity of solar radiation at the top of the atmosphere, and the angle (and hence pathlength) of light through the atmosphere. Light scattering in the atmosphere is not considered. At the sea surface, a fraction of the light is reflected, and the rest refracted (Kirk, 1994). The pathlength of the beam through the water medium is calculated from the refracted angle, and a correction made [equations (23–26)] to account for scattering within the water. Nitrate was assumed to be the only limiting nutrient species, with a concentration below the mixed layer of $N_b = 2$ and 12 mol m^{-3} at Bermuda and OWS 'India', respectively. A summary of all the parameters used to specify environmental conditions appears in Table VIII.

Pigment concentrations and dimensions of eight phytoplankton species, and the dimensions, swimming velocity and feeding strategies of eight herbivore species are summarized in Tables IX, X and XII, respectively. Size-dependent general relationships are also given (Tables XIII and XIV). The model was run with just two phytoplankton species, *Skeletonema costatum* and *Phaeodactylum tricornutum*, and two spherical ($r = 10$ and 20 μm) herbivores based on general relationships. The phytoplankton species were chosen because of their common use in plankton studies. The cyanobacterial species were not chosen because of the order of magnitude increase in computational time resulting from the very dynamic behaviour of their internal quotas of nutrients: a result of having a large surface area to volume ratio. Herbivores based on general relationships were used because of the lack of data on yield and growth rates.

By simplifying K_z to a seasonally varying mixed layer and a fixed exchange rate with the water below the mixed layer, the model equations reduced to a system of ODEs. The ODEs are integrated forward in time using MATLAB with an adaptive step-size, 4th–5th order Runge–Kutta–Fehlberg integration scheme (Hoffman, 1992) requiring an accuracy on all state variables of:

Table VIII. Environmental parameter values and range for simulation of Bermuda Station 'S', 32°N and OWS 'India', 59°N. KE = kinetic energy. References: ϵ (Lazier and Mann, 1989); D_e, N_b (Strass and Woods, 1991; Taylor *et al.*, 1997); v, D_N (Li and Gregory, 1974); ρ_{water} (Pond and Pickard, 1983); b_w (Kirk, 1994); g_1, g_2 (Kirk, 1991). Refractive index of air/water interface = 1.341 (Kirk, 1994). Fundamental physical constants used (Atkins, 1994): Avogadro constant $A_v = 6.02214 \times 10^{23}$ mol^{-1}; Boltzmann constant $k_B = 1.38066 \times 10^{-23}$ J K^{-1}; Planck constant $h = 6.62608 \times 10^{-34}$ J s; Universal gas constant $R = 8.31451$ J K^{-1} mol^{-1}

Parameter	Symbol	Units	Bermuda	OWS India	Oceanic range
Mean dissipation of turbulent KE	ϵ	10^3 W m^{-3} = m^2 s^{-3}	10^{-7}		10^{-6}–10^{-9}
Nitrate below	N_b	mol m^{-3}	2×10^{-3}	12×10^{-3}	2–15×10^{-3}
Gravity	g	m s^{-2}	9.80665		± 0.02
Salinity	S	‰	35		33–37
Cloud fraction	C	otkas	4		0–8
Scattering coefficient of water	b_w	m^{-1}	0.05		0.02–0.3
Scattering coefficients	g_1	–	0.5		0.29–0.58
	g_2	–	0.2		0.13–0.23
Eddy diffusivity	D_e	m s^{-1}	6.66×10^{-6}		0.6–20×10^{-6}
Temperature	T	K	293	278	273–298
Molecular diffusivity of nitrate	D_N	m^2 s^{-1}	17.27×10^{-10}	13.44×10^{-10}	9.8–19×10^{-10}
Kinematic viscosity	v	m^2 s^{-1}	1.085×10^{-6}	1.394×10^{-6}	1.8–0.8×10^{-6}
Density of water	ρ_{water}	kg m^{-3}	1024.4	1026.6	1030–1000

Table IX. Scattering coefficient, b, and pigment concentrations in phytoplankton species. NS93, Nielsen and Sakshaug (1993); BDC96, Brunet *et al.* (1996); GOR85, Geider *et al.* (1985); K94, Kirk (1994); FDW85, Falkowski *et al.* (1985); JW94, Jeffery and Wright (1994); GHD92, Goldman *et al.* (1992); MAPVC93, Morel *et al.* (1993); ND, no data. Scattering coefficients from Morel and Bicaud (1986). If b for a species was unknown, diatoms were assumed to have $b = 0.5$ m^2 mg (Chl a)$^{-1}$ based on *S.costatum*, and cyanobacteria $b = 0.2$ m^2 mg (Chl a)$^{-1}$ based on *Synechocystis* sp.

Phytoplankton species	b [m^2 mg (Chl a)$^{-1}$]	Pigment concentrations [10^6 mg (pig) m^{-3}]				References
		Chl a	Chl b	Chl c	Carot.	
Skeletonema costatum	0.535	6.0	–	1.9	4.3	NS93,BDC96[a,b]
Phaeodactylum tricornutum	0.5	4.8	–	1.2	9.7	GOR85,K94[a,b]
Isochrysis galbana	0.066	4.3	–	1.3	5.1	FDW85,JW94[b]
Dictylum brightwelli	0.5	0.088	–	0.029	0.037	JW94[a,c]
Emiliania huxleyi	0.587	0.22	–	0.083	0.33	JW94[a]
Stephanopyxis palmeriana	0.5	0.30	–	0.064	ND	GHD92,JW94[d]
Synechococcus sp.	0.2	3.0	–	–	2.0	MAPVC93
Prochlorococcus marinus	0.2	9.4	8.2	–	3.6	MAPVC93

[a]Concentrations reported in mg (pig) cell^{-1}, and converted to mg (pig) m^{-3} using cell volume calculated from dimensions given in Table X.
[b]Accessory pigment concentration calculated from a separate study giving the ratio of the concentration of Chl a to accessory pigment.
[c]Using ratios of the molecular weight of Chl a and Chl c from Geider and Osbourne (1992).
[d]Using *Stephanopyxis turris* to determine Chl c concentration.

Table X. Taxa, shape and dimensions of phytoplankton species. PG75, Pasciak and Gavis (1975); SKA89, Sakshaug *et al.* (1989); WR97, Wolf-Gladrow and Riebesell (1997); FDW85, Falkowski *et al.* (1985); PCC, Plymouth Marine Laboratory (1990b); GHD92, Goldman *et al.* (1992); BW85, Bold and Wynne (1985); MAPVC93, Morel *et al.* (1993). Dimensions were obtained by: [2]all dimensions given in reference; [3]equivalent spherical diameter or volume given by first reference dimensions inferred by image in second reference; [4]equivalent spherical diameter given by reference, and without further information, shape assumed to be sphere; [5]ratio of radii assumed to be in direct proportion to *Synechococcus* sp.

Phytoplankton species	Taxa	Shape	r_1, r_2, r_3 (μm)	References
S.costatum	Diatom	Prolate	4, 2, 2	PG75,SKA89[2]
P.tricornutum	Diatom	Ellipsoid	12.5, 1.5, 1	WR97[2]
I.galbana	Haptophyte	Prolate	3.5, 1.9, 1.9	FDW85,PCC[3]
D.brightwelli	Diatom	Prolate	75, 25, 25	PG75[2]
E.huxleyi	Haptophyte	Sphere	5, 5, 5	PCC[4]
S.palmeriana	Diatom	Prolate	80, 32, 32	GHD92,BW85[3]
Synechococcus sp.	Cyanobacteria	Prolate	1.35, 0.27, 0.27	MAPVC93,BW85[3]
P.marinus	Cyanobacteria	Prolate	0.83, 0.17, 0.17	MAPVC93[5]

Table XI. Species-specific grazing yields. $Y_{j,k}^{-1}$, reciprocal of the grazing stoichiometry coefficient [cell (P_j) cell $(H_k)^{-1}$] calculated during exponential growth in batch culture. ND, no data; X, outside food range; B1, unidentified Gram-negative, motile, rod-shaped bacterium (0.8 × 1.4 × 1.8 μm) with a volume of ~0.67 μm^3; B2, *Escherichia coli* strain χ-1488, with assumed dimensions (0.6 × 0.6 × 0.6 μm) and volume 0.13 μm^3

$Y_{j,k}^{-1}$	B1	B2	*P.tricornutum*	*I.galbana*
Monosiga sp.[a]	ND	300	X	X
Ciliophrys marina[a]	ND	ND	X	X
Codosiga gracilis[b]	3989	ND	X	X
Favella sp.[a]	ND	ND	ND	ND
Paraphysomonas imperforata[a,b]	208	ND	78	34
Stephanoeca diplocostata[b]	733	ND	X	X
Bodo designis[b]	693	ND	X	X
Jakoba libera[b]	96	ND	X	X

References: [a]Shimeta *et al.* (1995); [b]Eccleston-Parry and Leadbeater (1994).

$$\text{Error} < 0.1 \min \begin{bmatrix} Q_{1,1}^{max} & \cdots & Q_{1,p}^{max} \\ \vdots & \cdots & \vdots \\ Q_{n,1}^{max} & \cdots & Q_{n,p}^{max} \end{bmatrix} \tag{62}$$

Phytoplankton populations were converted to units of mg (pig) m^{-3} by:

$$C_{T,b} = \sum_{j=1}^{p} C_{j,b} A_v P_j V_j \tag{63}$$

where $C_{T,b}$ is the total concentration of pigment b due to all phytoplankton cells.

A Bermuda simulation was run for 10 years, at which point it had reached a stable annual cycle, and results graphed for years 8, 9 and 10 (Figure 12). An India simulation was run for 40 years, without reaching a stable annual cycle. Years 18, 19 and 20 are graphed (Figure 13), as they are representative of the small amount

Table XII. Constants used to describe herbivore species. SJL95, Shimeta *et al.* (1995); EL94, Eccleston-Parry and Leadbeater (1994). Encounter mechanisms (Enc. mech.): RW, random walk, or diffusion; DI, direct interception, solved using rectilinear encounter rate coefficient; FF, filter feeder, solved using curvilinear encounter rate coefficient. Dimensions include any organic envelope (lorica) surrounding the cell. Dimensions were obtained by: [1]all dimensions given in reference; [2]equivalent spherical diameter or volume given by reference and dimensions inferred from schematic in reference; [3]equivalent spherical diameter given by reference, and without further information, shape assumed to be sphere. For FF, a volume clearance rate (m³ s⁻¹) given in the literature is converted to a product of a filter cross-sectional area (m²) [based on marked (*) dimensions] and a swimming velocity (m s⁻¹), and the swimming velocity is then used in the rectilinear coagulation formulae

Herbivore species	Shape	r_1, r_2, r_3 (μm)	Growth rate (d⁻¹)	Enc. mech.	Swim speed (μm s⁻¹)	Prey range (μm)	References
Monosiga sp.	sphere	3 3 3	1.6	FF	30	bacteria	SJL95[3]
C.marina	sphere	65 65 65	1.1[a]	RW	0	bacteria	SJL95[3]
Favella sp.	oblate	175 175 100	0.82	FF	1000	any algae	SJL95[1]
P.imperforata	sphere	4 4 4	5.0	DI	42	0.5–200	EL94[2]
S.diplocostata	cone	10 5* 5*	0.84	FF	178	bacteria	EL94[2]
B.designis	prolate	5 1.6 1.6	3.8	DI	80	bacteria	EL94[2]
J.libera	prolate	6 1.7 1.7	0.86	DI	19	bacteria	EL94[2]
C.gracilis	prolate	4 2.2* 2.2*	1.2	FF	215	bacteria	EL94[2]

[a]Growth rate based on *Ciliophrys infusionum* (Hansen *et al.*, 1997).

Table XIII. General relationships used to calculate size-dependent phytoplankton parameter values. V_j = volume of species j (m³); $Q_{N,j}^{max}$ = maximum internal quota of nitrate in species j; q_j^{max} = maximum internal quota of energy in species j; ρ_j = absolute density of species j; $U_{swim,j}$ = swimming velocity of species j; μ_j^m = maximum growth rate of species j; $E_{a,j}$ = activation energy of species j converted (Raven and Geider, 1988) from literature values of Q_{10} = ratio of reaction rates at $T + 10$ and T; $T_{ref,j}$ = temperature of maximum growth rate of species j; α_j = growth efficiency of species j; $m_{i,j}$ = stoichiometric ratio of reactant i in growth of species j; assumed to fit the Redfield ratio. $(C:Chl\ a)_j$ = molecular ratio of carbon to Chl a of species j

General relationship for phytoplankton	Units	Reference
$Q_{N,j}^{max} = 1.38 \times 10^3\ V_j$	mol (Q_N) cell⁻¹	Straile (1997)
$q_j^{max} = \dfrac{m_I}{m_N} Q_N^{max}$	mol (q) cell⁻¹	–
$\rho_j = \rho_{water} + 0.0369\ V_j^{-0.28}$	kg m⁻³	Kiørboe (1993)
$U_{swim,j} = 3.57 \times 10^{-3}\ V_j^{0.26/3}\ r^2 = 0.38$	m s⁻¹	Sommer (1988)
$\mu_j^m = 8.06 \times 10^{-8}\ V_j^{-0.15}\ r^2 = 0.34\ n = 126$	s⁻¹	Tang (1995)
$E_{a,j} = 5.4 \times 10^4\ (Q_{10} = 2.1)$	J mol⁻¹	Raven and Geider (1988)
$T_{ref,j} = T$	K	(Table VIII)
$\alpha_j = 0.75$	–	–
$m_I : m_C : m_N : m_P = 848 : 106 : 16 : 1$	–	Kirk (1994)
$m_{i,j} = A_v Q_{i,j}^{max}$	mol $(Q_{i,j})$ mol $(P_j)^{-1}$	–
$(C:Chl\ a)_j = 50$	–	Fasham *et al.* (1990)

of interannual variability that persisted throughout the simulation. In both simulations, the populations of *S.costatum* and the 10 μm herbivore persisted, while *P.tricornutum* and the 20 μm herbivore populations became vanishingly small. Interestingly, an India simulation run with only one phytoplankton species, *P.tricornutum*, produced a choatic (or periodicity > 40 years) output, but retained strong annual trends such as the spring bloom.
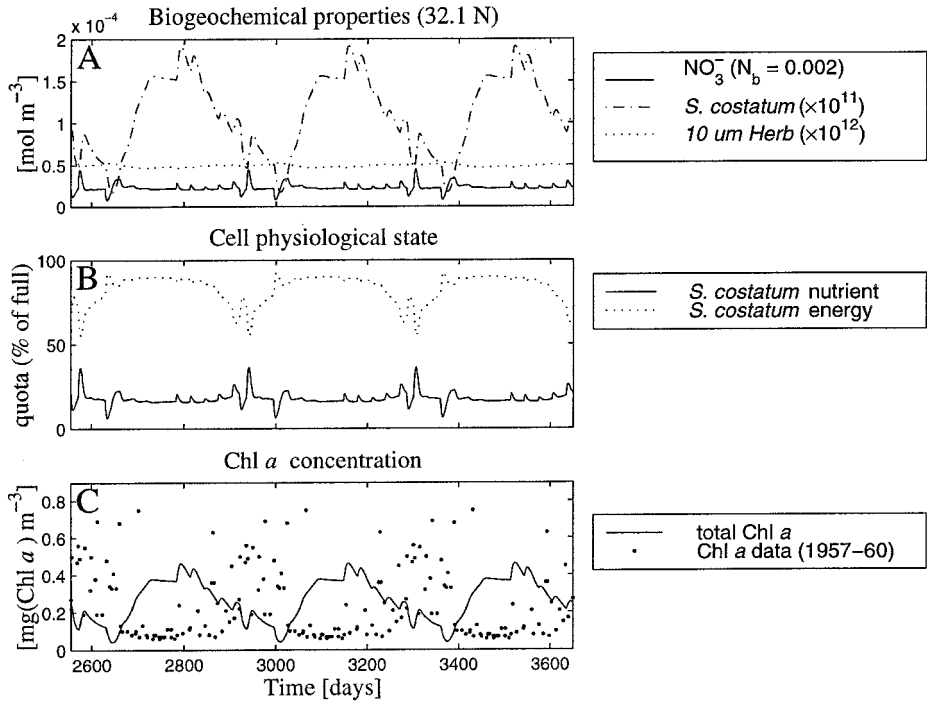
Fig. 12. Simulation of plankton population dynamics in the oceanic mixed layer at Bermuda (32°N, 65°W), graphing years 8, 9 and 10. (**A**) Nutrient and population dynamics: nitrate [mol (NO_3^-) m^{-3}]; phytoplankton [mol (cell) m^{-3}]; herbivores [mol (cell) m^{-3}]. (**B**) Dynamics of the physiological state of organisms, graphing internal nutrient quota, Q (% of Q^{max}), and energy quota, q (% of q^{max}). (**C**) Chl a concentration dynamics [equation (63)]. Note from (B) that nutrient is always more limiting than light.

Table XIV. General relationships used to calculate size-dependent herbivore parameter values. V_k = volume of species k (m^3); $U_{swim,k}$ = swimming velocity of species k; μ_k^m = maximum growth rate of species k; $E_{a,k}$ = activation energy of species k converted (Raven and Geider, 1988) from literature values of Q_{10} = ratio of reaction rates at $T + 10$ and T; $T_{ref,k}$ = temperature of maximum growth rate of species k; ρ_k = density of species k

General relationship for herbivores	Units	Reference
$\rho_k = \rho_{water}$	kg m^{-3}	–
$\mu_k^m = 2.40 \times 10^{-8}\ V_k^{-0.21}\ r^2 = 0.69\ n = 69$	s^{-1}	Hansen *et al.* (1997)
$Y_{j,k} = 0.33\ \dfrac{V_j}{V_k} \pm 0.032$ SE $n = 33$	predator prey^{-1}	Hansen *et al.* (1997)
$U_{k,swim} = 1.97 \times 10^{-2}\ V_k^{0.20}\ n = 39$	m s^{-1}	Hansen *et al.* (1997)
$E_{a,k} = 7.1 \times 10^4\ (Q_{10} = 2.8)$	J mol^{-1}	Hansen *et al.* (1997)
$T_{ref,k} = T$	K	(Table VIII)

Discussion

Choice of plankton interactions

The model equations (Table VII) do not contain a number of processes that are typically included in plankton population studies. Fasham *et al.* (1990), for
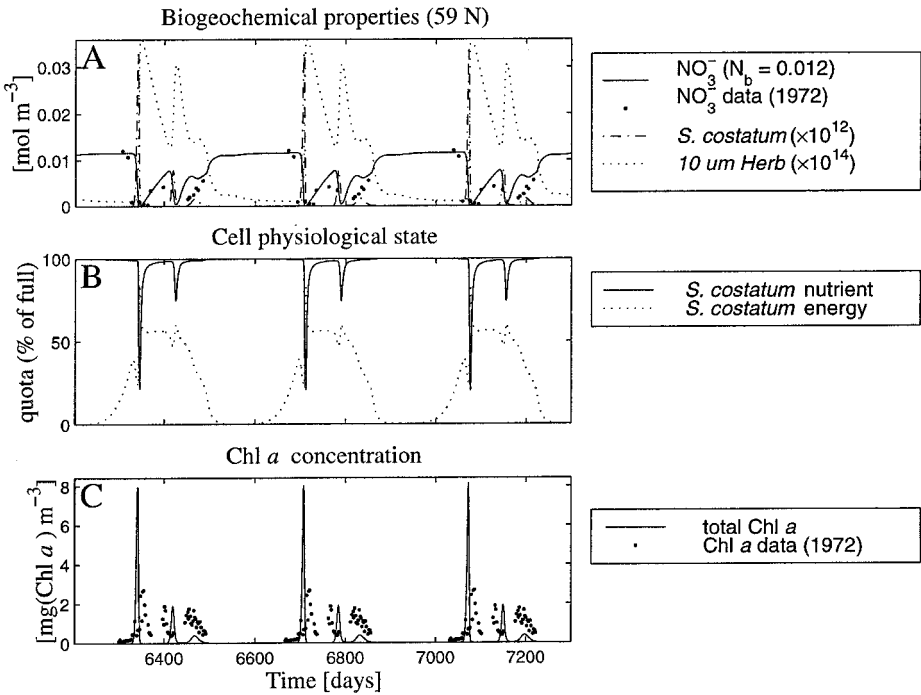
Fig. 13. Simulation of plankton population dynamics in the oceanic mixed layer at OWS 'India' (59°N, 19°W), graphing years 18, 19 and 20. (**A**) Nutrient and population dynamics: nitrate [mol (NO_3^-) m^{-3}]; phytoplankton [mol (cell) m^{-3}]; herbivores [mol (cell) m^{-3}]. (**B**) Dynamics of the physiological state of organisms, graphing internal nutrient quota, Q (% of Q^{max}), and energy quota, q (% of q^{max}). (**C**) Chl a concentration dynamics [equation (63)]. Note from (B) that light is always more limiting than nutrient, except during the spring bloom.

example, have detrital, dissolved organic nitrogen and bacteria state variables, and include processes of respiration, regeneration and mortality in their description of phytoplankton and zooplankton. Furthermore, theoretically analysed plankton processes described in the literature, but not utilized in this paper, include: sinking of biological populations, as a function of formation rates of 'marine snow' (Jackson, 1995); intra-species interactions, behaviours, histories or adaptations (McGillicuddy, 1995); action of pathogens (Suttle *et al.*, 1990) or chemical toxicity (Sunda and Huntsman, 1996) on biological populations; scavenging of microscopic organisms by aeration, and transport to the atmosphere (Blanchard, 1989); spatial heterogeneity of plankton populations (Piontkovski *et al.*, 1997); more complicated food chains including carnivores and cannibals (Fasham *et al.*, 1990) or mixotrophs (Raven, 1997); organization of fluid mixing such as Langmuir cells (Bees *et al.*, 1998); and internal cell processes (Flynn *et al.*, 1997).

Simply, it was decided to include only the most basic and well-understood processes required to formulate a plankton population model. Inclusion of processes which could not be constrained by physical laws would make it difficult to assess the value of the theoretical approach adopted in this paper. For example, a theoretical understanding of mixing and grazing processes allows a reasonable

estimate of resulting phytoplankton loss terms. However, estimates of another phytoplankton loss term, cell mortality, are poorly constrained. By not including poorly estimated processes, the simulation assesses whether the present theoretical understanding of plankton processes is sufficient to model plankton population dynamics.

Considerations of scale

The model equations have been formulated at the scale of the individual plankton cells. It is not possible to use the theoretical approach of this paper on larger scales such as phytoplankton biomass. Of course, there are a variety of scales smaller than the cell that could have been chosen (i.e. cell organelles, molecules, atoms, etc.). A quick comparison follows of the outputs of some of the mechanistic functional forms based on the individual to the output from functional forms based on a variety of smaller scales.

For light capture, the packaging of pigments into chloroplasts within cells has the potential to decrease light capture compared to the assumed uniform concentration of pigment within the cell. To test this, a hypothetical cell, A, of uniform pigment concentration can be compared to another cell, B, with the same quantity of pigment packaged into only one-third of the cell volume, although this one-third is spread evenly throughout the cell. Taking a sphere ($r = 5$ μm) with average Chl a concentration 10^6 mg (Chl a) m^{-3}, analysing a light beam of λ = 435 nm (Chl a's peak absorbance) and intensity $I_{incident}$ = 100 W m^{-2}: $\overline{\gamma C}_{A,435}$ = 7.59 × 10^4 m^{-1} [equation (16)]; $\overline{aA}_{A,435}$ = 3.04 × 10^{-11} m^{-2} (Table IV), so $I_{A,attenuated}$ = 3.04 × 10^{-9} W [equation (17)]. For cell B [which would attenuate light at the same rate as a sphere $r = 5 \sqrt[3]{1/3}$ μm, average Chl a concentration = 3 × 10^6 mg (Chl a) m^{-3}], $\overline{\gamma C}_{B,435}$ = 2.28 × 10^5 m^{-1}; $\overline{aA}_{B,435}$ = 2.36 × 10^{-11} m^{-2} and $I_{B,attenuated}$ = 2.36 × 10^{-9} W, a 30% difference. For a sphere, $r = 1$ μm, but otherwise the same parameters as above, the difference is only 6%. The larger, more spherical, more concentrated pigments are within the cell, and the higher $\overline{\gamma C}$, the worse the approximation of uniform pigment distribution becomes. For the purposes of this study, using primarily small phytoplankton cells, and considering light absorbed over the whole photosynthetic band, the choice of the individual as the scale of light capture is sufficient.

For nutrient uptake by diffusion, it has been shown (Berg and Purcell, 1977) that the number and distribution of nutrient uptake sites on a cell surface are such that the assumption of uniform cell wall concentration (and hence the individual as the smallest necessary scale) used in calculating nutrient flux is justified for algal cells. For convective fluxes, the correlations used (Table III) are based on whole particles, and can only be used to determine the average convective flux to the whole cell surface.

Choosing the individual as the scale for the 'chemical reaction' of growth cannot be verified in as simple a manner as for the mechanistic functional forms above. Nonetheless, it allows use of internal quotas with mechanistic uptake rates, and appears to capture much of the behaviour of cell populations. Mechanistic functional forms for encounter and sinking rates are clearly based on the

assumption that the individual is the relevant scale, and cannot be easily formulated on a different scale. A significant disadvantage of choosing the scale of the individual is that the processes modelled occur at small time scales. For example, it can take only minutes for a phytoplankton cell to become nutrient saturated, so the maximum time step in the numerical integration must be an equivalent size. Despite the resulting increase in computation time, the individual appears to be a good choice of scale for modelling plankton population dynamics.

The mechanistic functions

Functions which describe underlying physical mechanisms should provide better estimates of the rates of plankton interactions. Parameters determined in controlled laboratory environments are likely to be both more accurate and more precise than field estimations and, in general, physical parameters can be estimated more accurately and more precisely than biological parameters. When compared to non-mechanistic functional forms, mechanistic functional forms are typically based on a higher proportion of physical parameters than biological parameters. Furthermore, at the chosen scale of the individual cell, the source of parameter values inevitably becomes the laboratory. Since the laboratory environment (such as a chemostat) is still large compared to the organism, laboratory constants for use in mechanistic functional forms are applicable to field environments. This is not necessarily true of physical processes in the ocean, such as mixing, which occurs on a range of scales, some many orders of magnitude bigger than laboratory flows. Ironically, it may turn out that the modelling strategy of using mechanistic functional forms and laboratory-determined constants is better suited to biological models than physical models of the oceans.

From the above arguments, it should be expected that mechanistic functional forms will be more constrained than non-mechanistic functional forms. As an example, the nutrient uptake term [equation (15)] contains three laboratory-determined physical constants (ψ, D and Sh) and one laboratory-determined biological parameter (Q^{max}), while the more commonly applied Michaelis–Menten uptake term [equation (11)] has two field-determined biological parameters (V and K). D is known to three decimal places (Li and Gregory, 1974), ψ is exact for a known cell geometry, and for cell geometries for which Sh has been measured or theoretically derived Sh is $\pm$ 10%. Laboratory measurements of Q^{max} are also likely to be within 10%. Non-mechanistic, biomass models rely on field estimates of V and K which have literature values varying by a factor of 5 and 10^4 (Yool, 1997), respectively.

Much of the variation in field-determined biological parameters such as V is a result of the inability of non-mechanistic functional forms to include explicitly the effects of environmental conditions on the processes they describe (the other main source of uncertainty being sampling logistics). Mechanistic functions allow a more complete description of the effects of environmental factors on plankton than would a biomass model. Examples of this include: (i) the effect of small-scale turbulence being incorporated into nutrient uptake and grazing using Sh and ϕ, respectively;

(ii) the variation in 'particle effect' (Kirk, 1994) due to different wavelengths of light in the environment; and (iii) the effect of temperature on molecular diffusivity and viscosity being included in nutrient uptake and encounter rates.

Realizing the advantages of mechanistic functions relies on the correct application of physical laws, and significantly increased computing power. While computing power is expected to continue to increase, few mechanistic forms have been tailored specifically for plankton population dynamics, and gaps exist in the presented mechanistic model. In particular, the presented mechanistic theory of plankton interaction rates is incomplete for: determination of the encounter rate coefficient, ϕ, for non-spherical plankters; Sherwood numbers, Sh, for non-spherical plankters in shear and turbulent flows; and consideration of the effect of swimming methods on the local flow field.

Comparison with data, Fasham et al. *(1990) and Fasham (1993)*

The model presented has similar solar irradiance (albeit spectrally resolved) and mixing functions as Fasham *et al.* (1990) and Fasham (1993). However, while the Fasham models use empirical function forms based on field-measured (or estimated) parameters to describe plankton interactions, the presented model uses primarily mechanistic functional forms based on laboratory-determined parameters, sourced from studies performed independently of the modelling exercise. The simplification of the mixing equations [equations (52) and (53)] to ODEs resulted in a single environment. Given a single environment, it is not surprising that only one species of phytoplankton and herbivore persisted. In the real ocean, light, nutrient and turbulence vary in both the horizontal and vertical directions. The world's oceans contain thousands of plankton species. Simulations with space resolved at least vertically will be required to assess whether a mechanistic model such as the one presented can sustain a large variety of plankton species. Interestingly, another result of using a zero-dimensional model was that light capture by phytoplankton cells became independent of either the angle of light propagation through the water column, or the scattering characteristics. This is due to light being 'limiting' only in the winter, when light out of the mixed layer is small compared to the incident light on the upper surface of the layer, and is only negligibly decreased by an increase in pathlength due to scattering or azimuth angle.

OWS India simulation. The Fasham (1993) model OWS India simulation was compared to data from 1972 [Figure 10 in Fasham (1993)], part of a 5 year time series (Plymouth Marine Laboratory, 1990a). The 5 year data set showed considerable yearly variation in the size and frequencies of plankton blooms. The presented model (Figure 13) and Fasham (1993) appeared to capture much of the behaviour of phytoplankton and nutrient dynamics, although only the simulation run using only one phytoplankton species, *P.tricornutum*, showed significant yearly changes in size and frequency of plankton blooms.

Bermuda. The Fasham *et al*. (1990) model Bermuda simulation was compared to

data from 1958–60 [Figure 5 in Fasham *et al.* (1990)]. Neither the presented model (Figure 12) nor the Fasham *et al.* (1990) model captured the seasonal variation in nitrate or phytoplankton population. Both models overestimated the summer chlorophyll concentrations. This may be a result of the existence of deep-chlorophyll maxima in low latitudes, or horizontal advection associated with the Gulf Stream, phenomena which cannot be modelled with a zero-dimensional model. At Bermuda, where loss of scalars such as herbivores is less than at OWS India, introduction of an additional loss term to herbivores, such as cell mortality, sinking or vertical migration, may improve the simulation. Introduction of such terms into a mechanistic model, however, would require a better understanding of the underlying processes involved.

For the oceanic mixed layer at Bermuda and OWS India the presented model performance was similar to the Fasham models. This result was achieved with a model based on primarily laboratory-determined constants, and a small number of well-constrained environmental parameters (Table VIII). Of the environmental parameters, only the deep water nutrient concentration, $N_{i,b}$, would not be an output of a three-dimensional coupled atmospheric–ocean turbulent closure mixing model forced by a spectrally resolved solar radiation algorithm. Considering the variety of oceanic environments, and the costs of field sampling programmes, a model based almost entirely on laboratory-determined constants rather than field-determined parameters may be able to justify the significant number of laboratory experiments (to obtain parameters from a wider variety of marine plankton species) and computational overheads (required to run three-dimensional models), which make such a three-dimensional mechanistic model simulation more costly than a simple empirical plankton population model simulation.

In conclusion, this paper has worked towards a plankton population model constructed using mechanistic functional forms only. The mechanistic approach necessitated the modelling of plankton interactions on the scale of individual plankton cells, and inevitably led to the use of laboratory-determined constants. This appears to provide a way around the problem of uncertainties in field-determined parameters and arbitrary choices of functional forms that reduce the predictive power of many plankton models. The model is ideally suited to being coupled to a multi-layer turbulent closure mixing model. Such a coupled model, though computationally intensive, would only require inputs of deep water nutrient concentrations, laboratory-determined constants and an initial variety of plankton species.

Acknowledgements

References

Atkins,P.W. (1994) *Physical Chemistry*, 5th edn. Oxford University Press, Oxford.

Bees,M.A., Mezić,I. and McGlade,J.M. (1998) Planktonic interactions and chaotic advection in Langmuir circulation. *Math. Comput. Simulation*, **44**, 527–544.

Berg,H.C. and Purcell,E.M. (1977) Physics of chemoreception. *Biophys. J.*, **20**, 193–219.

Blake,J.R. and Otto,S.R. (1996) Ciliary propulsion, chaotic filtration and a 'blinking' stokeslet. *J. Eng. Math.*, **30**, 151–168.

Blanchard,D.C. (1989) The ejection of drops from the sea and their enrichment with bacteria and other materials: a review. *Estuaries*, **12**, 127–137.

Bold,H.C. and Wynne,M.J. (1985) *Introduction to the Algae*, 2nd edn. Prentice-Hall, Inc., New Jersey.

Botsford,L.W., Castilla,J.C. and Peterson,C.H. (1997) The management of fisheries and marine ecosystems. *Science*, **277**, 509–515.

Brenner,H. (1963) Forced convection heat and mass transfer at small Peclet numbers from a particle of arbitrary shape. *Chem. Eng. Sci.*, **18**, 109–122.

Bricaud,A., Morel,A. and Prieur,L. (1981) Absorption by dissolved organic matter of the sea (yellow substance) in the UV and visible domains. *Limnol. Oceanogr.*, **26**, 43–53.

Brock,T.D. (1981) Calculating solar radiation for ecological studies. *Ecol. Modelling*, **14**, 1–19.

Brunet,C., Davoult,D. and Casotti,R. (1996) Physiological reactions to a change in light regime in cultured *Skeletomena costatum* (Bacillariophyta): implications for estimation of phytoplankton biomass. *Hydrobiologia*, **333**, 87–94.

Clary,D.C. (1998) Quantum theory of chemical reaction dynamics. *Science*, **279**, 1879–1882.

Clift,R., Grace,J.R. and Weber,M.E. (1978) *Bubbles, Drops and Particles*. Academic Press, New York.

Dabros,T., Adamczyk, Z. and deVen,T.G.M.V. (1984) Transfer of colloidal particles to a cylinder in combined simple shear and uniform flow. *Physio Chemical Hydrodyn.*, **5**, 67–83.

de Baar,H.J.W. (1994) Von Liebig's law of the minimum and plankton ecology (1899–1991). *Prog. Oceanogr.*, **33**, 347–386.

Dower,J.F., Miller,T.J. and Leggett,W.C. (1997) The role of microscale turbulence in the feeding ecology of larval fish. *Adv. Mar. Biol.*, **31**, 169–220.

Driscoll,W.G. and Vaughan,W. (1978) *Handbook of Optics*. McGraw-Hill, New York.

Droop,M.R. (1968) Vitamin B-12 and marine ecology IV. The kinetics of uptake, growth and inhibition in *Monochrysis lutheri. J. Mar. Biol. Assoc. UK*, **48**, 689–733.

Dugdale,R.C. (1967) Nutrient limitation in the sea: dynamics, identification and significance. *Limnol. Oceanogr.*, **12**, 685–695.

Dyhrman,S.T. and Palenik,B.P. (1997) The identification and purification of a cell-surface alkaline phosphatase from the dinoflagellate *Prorocentrum minimum* (Dinophyceae). *J. Phycol.*, **33**, 602–612.

Eccleston-Parry,J.D. and Leadbeater,B.S.C. (1994) A comparison of the growth kinetics of six marine heterotrophic nanoflagellates fed with one bacterial species. *Mar. Ecol. Prog. Ser.*, **105**, 167–177.

Edwards,A.M. and Brindley,J. (1996) Oscillatory behaviour in a three-component plankton population model. *Dynam. Stabil. Syst.*, **11**, 347–370.

Falkowski,P.G., Dubinsky,Z. and Wyman,K. (1985) Growth-irradiance relationships in phytoplankton. *Limnol. Oceanogr.*, **30**, 311–321.

Fasham,M.J.R. (1993) Modelling the marine biota. In Heimann,M. (ed.), *The Global Carbon Cycle*. Springer-Verlag, New York, pp. 457–504.

Fasham,M.J.R., Ducklow,H.W. and McKelvie,S.M. (1990) A nitrogen-based model of plankton dynamics in the oceanic mixed layer. *J. Mar. Res.*, **48**, 591–639.

Flynn,K.J., Fasham,M.J.R. and Hipkin,C.R. (1997) Modelling the interactions between ammonium and nitrate uptake in marine phytoplankton. *Philos. Trans. R. Soc. London Ser. B*, **352**, 1625–1645.

Geider,R.J. and Osbourne,B.A. (1992) *Algal Photosynthesis*. Chapman and Hall, New York.

Geider,R.J., Osbourne,B.A. and Raven,J.A. (1992) Light dependence of growth and photosynthesis in *Phaeodactylum tricornutum* (Bacillariophyceae). *J. Phycol.*, **21**, 609–619.

Geider,R.J., MacIntyre,H.L. and Kana,T.M. (1997) Dynamic model of phytoplankton growth and acclimation: responses of the balanced growth rate and the chlorophyll *a*:carbon ratio to light, nutrient-limitation and temperature. *Mar. Ecol. Prog. Ser.*, **148**, 187–200.

Gerritsen,J. and Strickler,J.R. (1977) Encounter probabilities and community structure in zooplankton: a mathematical model. *J. Fish. Res. Board Can.*, **34**, 73–82.

Goldman,J.C., Hansell,D.A. and Dennett,M.R. (1992) Chemical characterization of three large oceanic diatoms: potential impact on water column chemistry. *Mar. Ecol. Prog. Ser.*, **88**, 257–270.

Hansen,P.J., Bjornsen,P.K. and Hansen,B.W. (1997) Zooplankton grazing and growth: Scaling within the 2–2,000 μm body size range. *Limnol. Oceanogr.*, **42**, 687–704.

Hill,R. and Whittingham,C.P. (1955) *Photosynthesis*. Methuen, London.

Hoepffner,N. and Sathyendranath,S. (1991) Effect of pigment composition on absorption properties of phytoplankton. *Mar. Ecol. Prog. Ser.*, **73**, 11–23.

Hoffman,J.D. (1992) *Numerical Methods for Engineers and Scientists*. McGraw-Hill, New York.

Jackson,G.A. (1995) Coagulation of marine algae. In Huang,C.P., O'Melia,C.R. and Morgan,J.J. (eds), *Aquatic Chemistry: Interfacial and Interspecies Processes*. American Chemical Society, Washington, DC, pp. 203–217.

Jackson,G.A. and Lochmann,S.E. (1992) Effect of coagulation on nutrient and light limitation of an algal bloom. *Limnol. Oceanogr.*, **37**, 77–89.

Jeffery, S.W. and Wright, S.W. (1994) Photosynthetic pigments in the haptophyta. In Green,J.C. and Leadbeater,B.S.C. (eds), *The Haptophyte Algae*. Clarendon Press, Oxford, pp. 111–132.

Karp-Boss,L., Boss,E. and Jumars,P.A. (1996) Nutrient fluxes to planktonic osmotrophs in the presence of fluid motion. *Oceanogr. Mar. Biol. Annu. Rev.*, **34**, 71–107.

Kennett,J.P. (1982) *Marine Geology*. Prentice-Hall, Inc., New Jersey.

Kerr,R.A. (1998) Models win big in forecasting El Niño. *Science*, **280**, 522–523.

Kiørboe,T. (1993) Turbulence, phytoplankton cell size, and the structure of pelagic food webs. *Adv. Mar. Biol.*, **29**, 1–72.

Kiørboe,T. *et al.* (1996) Sedimentation of phytoplankton during a diatom bloom: rates and mechanisms. *J. Mar. Res.*, **54**, 1123–1148.

Kirk,J.T.O. (1975a) A theoretical analysis of the contribution of algal cells to the attenuation of light within natural waters. I. General treatment of suspensions of pigmented cells. *New Phytol.*, **75**, 11–20.

Kirk,J.T.O. (1975b) A theoretical analysis of the contribution of algal cells to the attenuation of light within natural waters. II. Spherical cells. *New Phytol.*, **75**, 21–36.

Kirk,J.T.O. (1976) A theoretical analysis of the contribution of algal cells to the attenuation of light within natural waters. III. Cylindrical and spheroidal cells. *New Phytol.*, **77**, 341–358.

Kirk,J.T.O. (1981) A Monte Carlo study of the nature of the underwater light field in, and the relationship between optical properties of, turbid yellow waters. *Aust. J. Mar. Freshwater Res.*, **32**, 517–532.

Kirk,J.T.O. (1984) Dependence of relationship between inherent and apparent optical properties of water on solar altitude. *Limnol Oceanogr.*, **29**, 350–356.

Kirk,J.T.O. (1991) Volume scattering function, average cosines, and the underwater light field. *Limnol. Oceanogr.*, **36**, 455–467.

Kirk,J.T.O. (1994) *Light and Photosynthesis in Aquatic Ecosystems*, 2nd edn. Cambridge University Press, Cambridge.

Koller,L.R. (1965) *Ultraviolet Radiation*, 2nd edn. John Wiley and Sons, New York.

Kuchel,P.W. and Ralston,G.B. (1988) *Schuam's Outline of Theory and Problems of Biochemistry*. McGraw-Hill, Sydney.

Lazier,J.R.N. and Mann,K.H. (1989) Turbulence and the diffusive layers around small organisms. *Deep-Sea Res.*, **36**, 1721–1733.

Lewis,M.R., Ulloa,O. and Platt,T. (1988) Photosynthetic action, absorption, and quantum yield spectra for a natural population of *Oscillatoria* in the North Atlantic. *Limnol. Oceanogr.*, **33**, 92–98.

Li,Y. and Gregory,S. (1974) Diffusion of ions in sea water and in deep-sea sediments. *Geochim. Cosmochim. Acta*, **38**, 703–714.

Libes,S.M. (1992) *An Introduction to Marine Biogeochemistry*. John Wiley and Sons, New York.

Lohmann,H. (1902) Die coccolithophoridae, eine monographie der coccolith en bildenden flagellaten, zuglish ein beitrag zur kenntnis des mittelmeerauftriets. *Arch. Protistenkd.*, **1**, 89–165.

McGillicuddy,D.J. (1995) One-dimensional numerical simulation of primary production: Lagrangian and Eulerian formulations. *J. Plankton Res.*, **17**, 405–412.

Mellor,G.L. and Yamada,T. (1982) Development of a turbulent closure model for geophysical fluid problems. *Rev. Geophys. Space Phys.*, **20**, 851–875.

Mierle,G. (1985a) Kinetics of phosphate transport by *Synechococcus leopoliensis* (Cyanophyta): evidence for diffusion limitation of phosphate uptake. *J. Phycol.*, **21**, 177–181.

Mierle,G. (1985b) A method for estimating the diffusion resistance of the unstirred layer of microorganisms. *Biochim. Biophys. Acta*, **812**, 827–834.

Morel,A. and Bicaud,A. (1986) Inherent properties of algal cells including picoplankton: theoretical and experimental results. In Platt,T. and Li,W.K.W. (eds), *Photosynthetic Picoplankton. Can. Bull. Fish Aquat. Sci.*, **214**, 521–559.

Morel,A., Ahn,Y., Partensky,F., Vaulot,D. and Claustre,H. (1993) *Prochlorococcus and Synechococcus*: A comparative study of their optical properties in relation to their size and pigmentation. *J. Mar. Res.*, **51**, 617–649.

Nielsen,M.V. and Sakshaug,E. (1993) Photobiological studies of *Skeletonema costatum* adapted to spectrally different light regimes. *Limnol. Oceanogr.*, **38**, 1576–1581.

Pahlow,M., Riebesell,U. and Wolf-Gladrow,D.A. (1997) Impact of cell shape and chain formation on nutrient acquisition by marine diatoms. *Limnol. Oceanogr.*, **42**, 1660–1672.

Pasciak,W.J. and Gavis,J. (1975) Transport limited nutrient uptake rates in *Dictylum brightwellii. Limnol. Oceanogr.*, **20**, 604–617.

Piontkovski,S.A., Williams,R., Peterson,W.T., Yunev,O.A., Minkina,N.I., Vladimirov,V.L. and Blinkov,A. (1997) Spatial heterogeneity of the plankton fields in the upper mixed layer of the open ocean. *Mar. Ecol. Prog. Ser.*, **148**, 145–154.

Plymouth Marine Laboratory (1990a) *Ocean Weather Station India 1971–1975 Part I.* Natural Environment Research Council, Plymouth.

Plymouth Marine Laboratory (1990b) *Plymouth Culture Collection: List of Strains.* Natural Environment Research Council, Plymouth.

Pond,S. and Pickard,G.L. (1983) *Introductory Dynamical Oceanography*, 2nd edn. Pergamon, Oxford.

Raven,J.A. (1997) Phagotrophy in phototrophs. *Limnol. Oceanogr.*, **42**, 198–205.

Raven,J.A. and Geider,R.J. (1988) Temperature and algal growth. *New Phytol.*, **110**, 441–461.

Rothschild,B.J. and Osborn,T.R. (1988) Small-scale turbulence and plankton contact rates. *J. Plankton Res.*, **10**, 465–474.

Sakshaug,E., Andersen,K. and Kiefer,D.A. (1989) A steady state description of growth and light absorption in the marine planktonic diatom *Skeletonema costatum. Limnol. Oceanogr.*, **34**, 198–205.

Sharples,J. and Tett,P. (1994) Modelling the effect of physical variability on the midwater chlorophyll maximum. *J. Mar. Res.*, **52**, 219–238.

Shimeta,J., Jumars,P.A. and Lessard,E.J. (1995) Influences of turbulence on suspension feeding by planktonic protozoa; experiments in laminar shear fields. *Limnol. Oceanogr.*, **40**, 845–859.

Smith,F.A. and Walker,N.A. (1980) Photosynthesis by aquatic plants: effects of unstirred layers in relation to assimilation of CO_2 and HCO_3^- and to carbon isotopic discrimination. *New Phytol.*, **86**, 245–259.

Smith,S.D. and Dobson,F.W. (1984) The heat budget at Ocean Weather Station *Bravo. Atmosphere-Ocean*, **22**, 1–22.

Sommer,U. (1988) Some size relationships in phytoflagellate motility. *Hydrobiologia*, **161,** 125–131.

Steele,J.H. and Henderson,E.W. (1981) A simple plankton model. *Am. Nat.*, **117**, 676–691.

Stockdale,T.N., Anderson,D.L.T., Alves,J.O.S. and Balmaseda,M.A. (1998) Global seasonal rainfall forecasts using a coupled ocean-atmosphere model. *Nature*, **392**, 370–373.

Straile,D. (1997) Gross growth efficiencies of protozoan and metazoan zooplankton and their dependence on food concentration, predator–prey weight ratio, and taxonomic group. *Limnol. Oceanogr.*, **42**, 1375–1385.

Strass,V.H. and Woods,J.D. (1991) New production in the summer revealed by the meridional slope of the deep chlorophyll maximum. *Deep-Sea Res.*, **38**, 35–56.

Sunda,W.G. and Huntsman,S.A. (1996) Antagonism between cadmium and zinc toxicity and manganese limitation in a coastal diatom. *Limnol. Oceanogr.*, **41**, 373–387.

Suttle,C., Chan,A. and Cottrell,M. (1990) Infection of phytoplankton by viruses and reduction of primary productivity. *Nature*, **347**, 467–469.

Tang,E.P.Y. (1995) The allometry of algal growth rates. *J. Plankton Res.*, **17**, 1325–1335.

Taylor,A.H. and Stephens,J.A. (1993) Diurnal variations of convective mixing and the spring bloom of phytoplankton. *Deep-Sea Res. II*, **40**, 389–408.

Taylor,A.H., Geider,R.J. and Gilbert,F.J.H. (1997) Seasonal and latitudinal dependencies of phytoplankton carbon-to-chlorophyll *a* ratios: results of a modelling study. *Mar. Ecol. Prog. Ser.*, **152**, 51–66.

von Liebig,J. (1840) *Chemistry in its Application to Agriculture and Physiology*. Taylor and Walton, London.

Wolf-Gladrow,D. and Riebesell,U. (1997) Diffusion and reactions in the vicinity of plankton: a refined model for inorganic carbon transport. *Mar. Chem.*, **59**, 17–34.

Yool,A. (1997) The dynamics of open-ocean plankton ecosystem models. PhD Thesis, Department of Biological Sciences, University of Warwick.